Report: On the activities of the 1st and 2nd years of PhD activity

PhD Title- Single Photons On-Demand from a 2D Material Heterostructure.

Student:

Tiago Alves Queirós, ID9520

Supervisors:

Dr. rer. nat. Jana B. Nieder, INL- International Iberian Nanotechnology Laboratory in Braga, Portugal .

Prof. Dr. Pedro Alpuim, Department of Physics of UMinho and INL

Contents

Preamble

This report describes the progress accomplished and tasks performed so far in the first and second years of the PhD academic programme and the research project. The report is structured according to a research plan and communicates the advances made on material growth, characterisation, and fabrication of a controllable single-photon emitter device.

Introduction

Single-photon emitters (SPEs) are becoming one of the primary building blocks of future photonic technologies, as this fundamental resource would enable scalable fabrication of quantum information technologies. A perfect on-demand SPE should be capable of emitting singular photons with precision in time, indistinguishable from each other. Such a device would allow the implementation of several Quantum technologies such as Quantum computing schemes, Quantum secure communication protocols, and Quantum sensing and metrology[1]. SPEs are also often referred to as antibunched light sources, meaning that the light produced by said source follows sub-Poissonian statistics and is distinctly non-classical.

Graphene is a two-dimensional semi-metal whose Fermi level, and thus optical conductivity, can be altered in many ways, such as electrostatic gating, chemical doping, physical straining, etc[2]. By elevating or lowering the graphene's Fermi level, it is possible to manipulate its properties so it can control the passage of light via **Pauli blocking**[3], which consists in filling all the states in graphene up to a given energy level such that photoelectric transitions can no longer occur for photon energies inferior to the Fermi level.

The complementary crystal lattice matching between graphene and hBN[4] alongside graphene's light-switching capabilities may prove to be a **highly scalable** means of producing single-photon on-demand devices.

In this report, the progress accomplished in the first and second years of research on the topic of single photons on-demand from a 2D material heterostructure is

highlighted. A topic such as chemical vapour deposition of 2D materials, 2D material characterisation, fluorescence microscopy and probing of properties of single photon emitter (SPE) in hBN, as well as microfabrication of electrically controllable 2D material SPE platforms are addressed.

WP0: Academic Programme

The MAPfis doctoral programme in physics includes an academic curricular component that featured the following classes and seminars:

The following course elements are part of the Advanced Physics Topics I and will contribute to 12 ECTS points.

-Introduction to Nano-Optics: A tutorials based class where the student is tasked with writing and presenting a report on a Nano-Optics theme of their choosing. In this case the report was on the theme of how to bypass the optical diffraction limit of light using sub-wavelength light-matter interaction;

-Advanced Material Preparation and Characterisation: A series of classes on sample preparation and characterisation techniques such as sputtering, laser ablation, spectroscopic ellipsometry, Raman spectroscopy, x-ray diffraction, etc… The student was tasked with completing a written test about the subjects covered in the classes and writing a report on one of the techniques explained in the classes (in the case of this student the selected technique was Raman spectroscopy);

-Integration of Single-Photon Sources in Photonic Devices for Quantum Technologies: A tutorials based class requested by the student, as it pertains directly to his PhD topic. The student was tasked to conduct experiments with 2D material chemical vapour deposition and performing image processing analysis for the extraction and characterisation of single photon emitter time traces from hBN samples. A report based on the findings was delivered;

-Physics of Electronic Materials and Devices: A series of classes on semiconductor and condensed matter physics and some of its respective applications. The student was tasked to solve homework exercises on the subject.

-Communicating Science: A set of classes on how to prepare, train, and successfully deliver an oral presentation. The student was tasked with delivering a presentation explaining and introducing his PhD topic to a non-scientific audience in the restricted time frame of 3 minutes; (3 ECTS)

-Entrepreneurship: A series of classes introducing entrepreneurship methods and concepts on how to develop and evaluated a business plan. The student was tasked with brainstorming a business idea in a group and developing the business plan for the respective idea. A report, an oral presentation, and an analysis on an article pertaining to the topic of regional development was delivered; (3 ECTS)

-Defence of the Essay: A literature review of the state-of-the art and introduction to the PhD topic as well as an elaboration and justification of a work plan for the tasks to be undertaken during the PhD were reported. In addition, the essay was defended publicly in an oral presentation before a committee of MAPfis professors. (12 ECTS)

The academic program requires 30 approved ETCS points, thus, the candidate successfully achieved the academic requirements during the first year.

WP1: Fabrication of hBN, Graphene and hybrid devices

As indicated in the work plan delivered one year prior the first task consisted on the growth and preparation of the 2D materials necessary for the assembly of the 2D material heterostructure.

In the following the progress on these tasks will be described.

WP1.1. Materials

-WP1.1.1. Material growth

Continuous **hBN thin films** were prepared by **atmosphere pressure chemical vapour deposition (AP-CVD)**. Firstly, the catalytic substrates used in the growth process (99.99999% pure 2 by 10 cm^2 copper foil) were prepared by 1-minute chemical polishing in ultrasounds using a mixture of 10 mL of HCl (37%), 10 mL of $FeCl_3$, and 280 mL of pure water. The substrates were mounted on a silicon oxide/silicon holder and placed in a quartz tube, centred on the reaction furnace that surrounds the part of the tube where the growth reaction happens. Solid ammonia borane precursor (8.5 mg) is placed in an

aluminium crucible which is also mounted in the quartz tube part surrounded by a heater. Secondly, a flow of 100 sccm of Ar/H_2 (95%/5%) gas mixture is injected from one side of the tube for 20 minutes to purge the atmosphere of other potentially reactive gases, like oxygen. Then the substrate is annealed at 1020 °C for 40 minutes, taking the furnace 25 extra minutes to reach this temperature. Post-annealing, the substrate is cooled down to room temperature before the next step, which consists in heating the precursor at 100 °C for 150 minutes under a lower 5 sccm gas flow to sublimate the ammonia borane into gas precursors. After triggering the precursor's phase change, the furnace is once more heated to 1020 °C and a gas mixture flow of 100 sccm is injected to act as a carrier gas to the sublimated precursor, which will transport the reagents to the substrate where the hBN growth takes place over the course of 30 minutes after a 25 minute heating step.

Hexagonal Boron Nitride is highly regarded for being a host material for **room temperature** single photon emitters (SPEs)[5,6]. In line with the objective of assembling a 2D material heterostructure, graphene was transferred onto hBN to study the effects on the emission characteristics on the SPEs.

Graphene flakes and continuous graphene films were grown by **oxygen assisted low pressure chemical vapour deposition (LP-CVD)**. The 5 by 5 and 10 x 10 cm^2 copper foil substrates were treated with the same chemical polishing treatment as for the hBN growth process and were also oxidised on a hot plate at 250 °C for 30 minutes, to increase the oxygen concentration during growth. This substrate is mounted in a graphite box with a sapphire disk mounted over it using two graphite supports. The purpose of the sapphire is to continuously release oxygen during the reaction process which mediates the growth of large graphene crystals. The purpose of the graphite box is two-fold, it both confines the atmosphere near the sample to increase the oxygen concentration near the sample and protects the material from the deposition of silicates originating from the sublimation of the quartz tube reactor[7]. The copper foil is annealed in an argon atmosphere for 30 minutes at 1040 °C. Methane is injected as a precursor gas for graphene, along with argon to adjust the partial pressure of the reagents, and hydrogen which mediates the growth process in conjunction with the oxygen to enable the deposition of large crystals and large grain continuous graphene. The growth process is done at 1040 °C. Parameters such as methane, argon, and hydrogen flow, as well as

growth time and process pressure were varied to analyse their effects on the sample quality.

In conclusion the growth of the hBN and Graphene material was executed in line with the time plan proposed (First 8 months), and it should be highlighted that a considerably fast speed of fabrication of 30 min for over 1 mm sized graphene flakes was achieved[8]. The quality was enough to perform characterisation of functional properties described in WP2.

WP1.2. Devices

-WP1.2.1. Designs for 2D material heterostructure devices

Several strategies to assemble electrically addressable 2D material heterostructures for the controlled fluorescent quantum emission from hBN defects simultaneously using hBN as a gate dielectric for modulating graphene's Fermi level were implemented. The **first** attempt, illustrated in Figure 1, consisted of a simple manual stacking of graphene/hBN/graphene layers, where each graphene layer acted as a condenser plate which could be addressed using probe needles, and the hBN layer served as the dielectric.

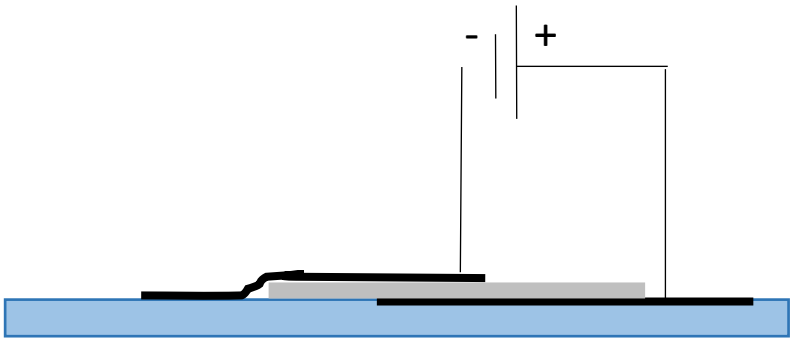

Figure 1: Illustration of the manually assembled stack of 2D materials. The black lines illustrate graphene and the grey layer illustrates the hBN containing SPEs

The **second** strategy involved microfabrication in assembling metal contacts to facilitate ohmic contact to the graphene layers without damaging the 2D materials and patterning the heterostructure into 7 by 5 mm^2 areas.

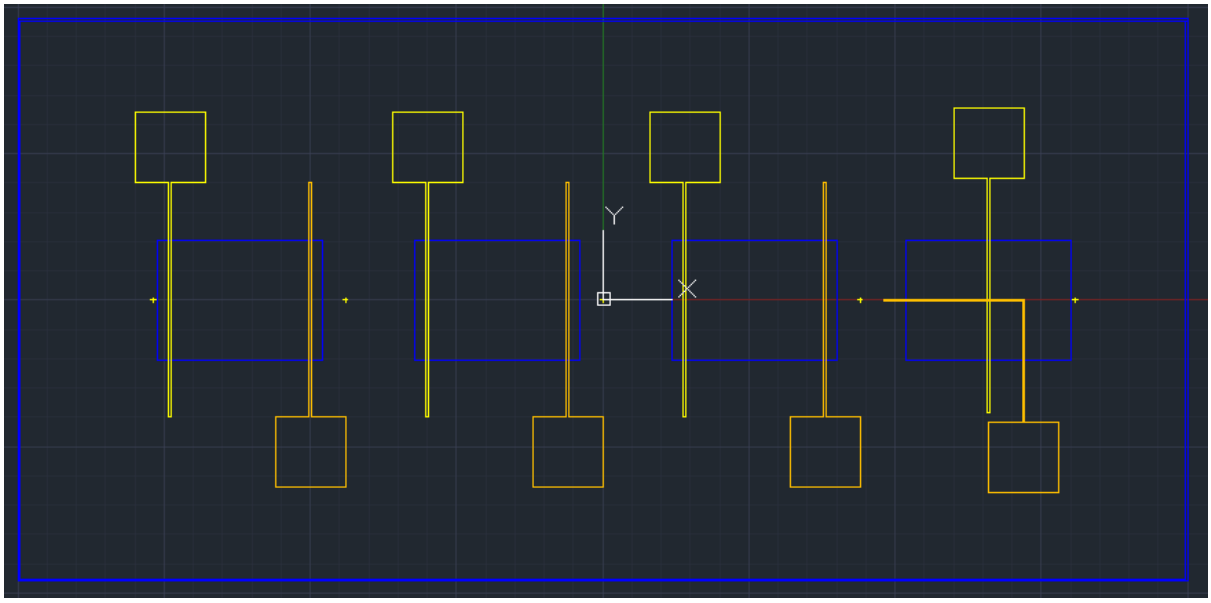

Figure 2: Schematic of the lithography masks used in the devices' microfabrication. The yellow layer represents the metal contacts addressing the bottom graphene layer, the blue rectangles represent the 2D material heterostructure etch protection mask, and the orange mask represents the metal contacts addressing the top graphene layer.

The **third** strategy consisted in replicating the previous process, but with microscopic-sized heterostructures and some variety in the design, such as 150 by 150 μm^2 graphene/hBN/graphene heterojunctions, 100 by 100 μm^2 graphene/hBN/graphene heterojunctions, and 150 by 150 μm^2 gold/hBN/graphene heterojunctions.

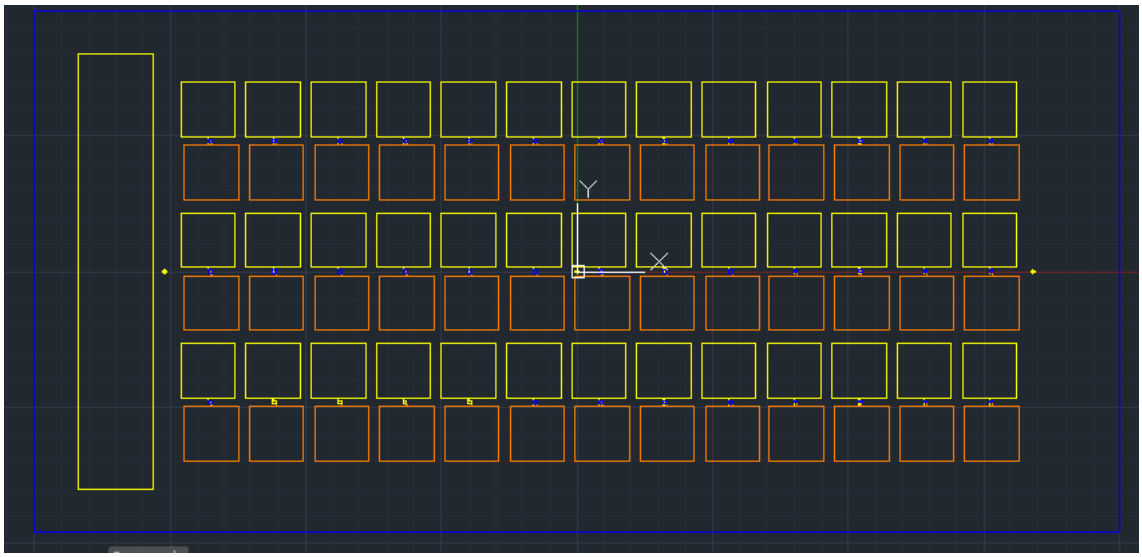

Figure 3: Schematic of the lithography masks used in the fabrication of the micro-heterostructures. The yellow mask represents the metal contacts addressing the bottom

graphene layers and a reference mass, the blue mask represents the heterostructures, and the orange mask represents the metal contacts addressing the top graphene layers

-WP1.2.2. Processes for fabrication

The manual stacking of 2D materials was done by multiple **polymer-assisted wet transfers of 2D materials**, a staple process in all devices implemented[9]. A layer of low molecular weight PMMA is deposited over the graphene or hBN layer by spin coating, and the opposite side of the copper foil, which holds the sample, is cleaned of 2D material residues with an oxygen plasma. The copper foil is etched at room temperature in 0.5 M $FeCl_3$ for approximately 3 hours to release the PMMA and graphene, or PMMA and hBN layers. The resulting membrane is then transferred to a low concentration (2%) HCl for 1 hour and 30 minutes to remove $FeCl_3$ residues from the 2DM's surface. After letting the sample rest for 10 minutes in a pure water bath, it is finally transferred to a glass coverslip and dried on a hotplate at 65 °C for 30 minutes. The removal of the PMMA is done overnight in an acetone bath. Finally, the samples are immersed in IPA and water to remove acetone residues.

The samples requiring microfabrication were assembled by combining the 2DM transfer process with **standard cleanroom processes** such as direct laser writing, spin coating, metal sputtering, and reactive ion etching.

To fabricate the bottom metal contacts, 1035 nm of AZ1505 positive photoresist were spin coated onto a HDMS primed glass coverslip. Direct laser writing was then used to pattern the bottom contact design on the photoresist, which was then developed using AZ400K. A metal stack of Cr/Au (3/10 nm) was deposited via magnetron sputtering, and the contacts were formed by liftoff in an acetone bath with ultrasounds. The 2D material heterostructure stack is then transferred using the same polymer-assisted wet transfer method. Another lithography exposure was done to pattern etch protection masks over the heterostructure region, and the surrounding 2DM was etched using inductively coupled oxygen plasma. Finally, another lithography cycle was done to form the top metal contacts by repeating the steps for the bottom contacts, except the final liftoff was done without ultrasounds to avoid damaging the graphene and hBN.

The micro heterostructure devices were fabricated using the same process, except for an additional graphene patterning to form the gold/hBN/graphene devices, and the top contact lithography was performed using a LOR + AZ1505 photoresist (500 nm/1035 nm) and an mr-Rem 500 solvent at 65 °C for the liftoff.

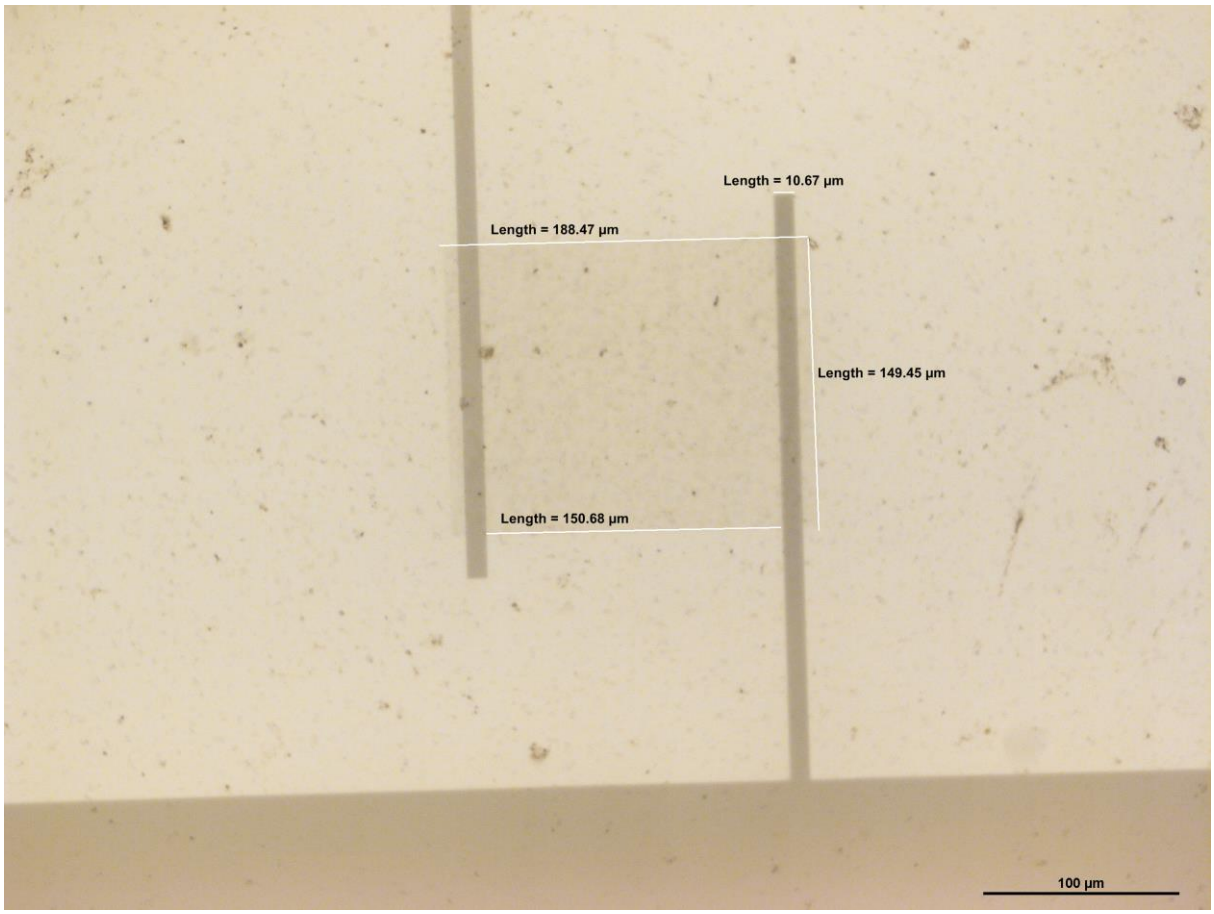

Figure 4: Example of a micro-fabricated graphene/hBN/graphene heterostructure with device area of 150 by 150 µm^2. The area surrounding the heterostructure is dirtied by debris formed during the 2D material etching step.

In conclusion, all three strategies using CVD hBN as the gate dielectric in a device that modulates the graphene's Fermi level failed to produce a usable device. However, much knowledge was obtained on proceeding and handling the 2D materials for future device designs. With the first strategy, it became evident that it would be impossible to achieve preliminary measurements without microfabrication. The second strategy revealed that the irregularity of the manual 2D material transfer method paired with large heterostructure sizes would result in short-circuited devices due to tearing in the insulator material and the higher likelihood of current transmission through pinholes in the material. The third strategy showed that even with shorter areas, the thinness of the

hBN layer would render the application of sufficient voltage difference to the graphene impossible without breaking down the material and short-circuiting the device.

Despite all the process sequences failing at producing functioning devices, this can be mainly attributed to the manual handling of the 2D materials, clipping of the material at the contact edges, and thinness of the hBN layer[10]. The standard cleanroom techniques were successfully implemented in patterning the 2D material heterostructure and forming metal contacts to address the graphene patches electrically.

-WP1.2.3. Assembling a device for electrostatic modulation of graphene

A new strategy to control the Fermi level of graphene in the vicinity of hBN had to be implemented with an independent gate dielectric since applying an electrostatic field through the CVD hBN quickly led to the hBN dielectric breakdown. The logical progression was to perform the gating of the graphene using a separate device and then place the hBN close to the graphene. This new attempt posed a new challenge because the microscopes at INL use an inverted geometry, which means that the materials selected for the fabrication of the device must be sufficiently transparent for efficient sample excitation and signal collection through the entire device. The concept for the device is comparable to a capacitor where the top plate is the graphene sheet, and the bottom plate, separated from the graphene by a dielectric, would be a transparent conductor. The device was made by sputtering 20 nm of Indium-Tin-Oxide (ITO) on a 170 µm thick glass coverslip and then performing optical lithography and liftoff to open a via on a subsequently sputtered 50 nm thick film of Al_2O_3. A layer of chromium and gold (3/20 nm) was sputtered over the sample, and a photoresist protection mask was patterned over the gold, shapping the device contacts. Ion milling using an ion beam at a fixed angle of 175° was performed to etch the surface metal into the shape of the contacts while providing a smooth incline for the 2D materials to attach to. (Figure 5)

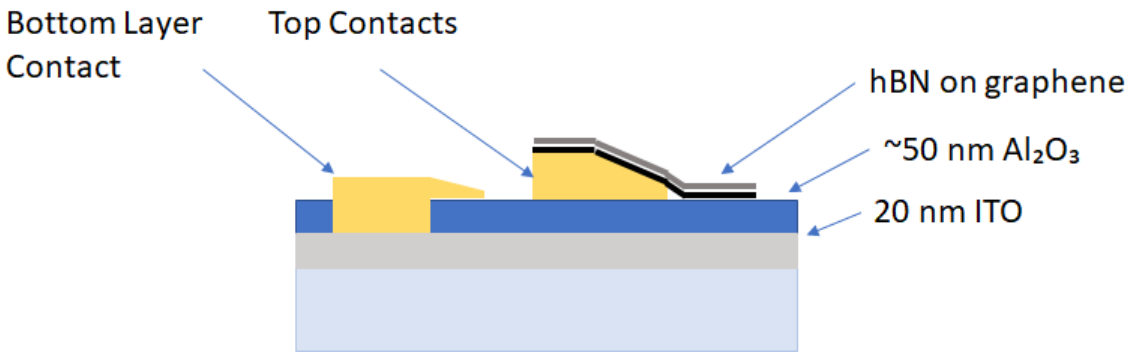

Figure 5: Illustration of a cross-section of the graphene Fermi level modulating device

The ion mill at a fixed angle was shown to lack homogeneity, and the large size selected for the probe needles' contact pads (1 x 1 mm^2) led to quick dielectric breakdown, such that the devices short-circuited before observing the desired fluorescence quenching and Pauli blocking effects during optical measurements. It became clear that adjustments had to be made regarding the contact patterning and dimensions.

WP2: Graphene and hBN Material characterisation

-WP2.1. Morphological characterisation

To **characterise the graphene flake morphology**, the samples were heated at 80 ° for 1 to 5 minutes to oxidise the copper foils substrate. Since substrate areas covered in graphene area protected from oxidation, this yields a very noticeable contrast between the graphene and the substrate[11]. Flake shape and size are then observed on the optical microscope.

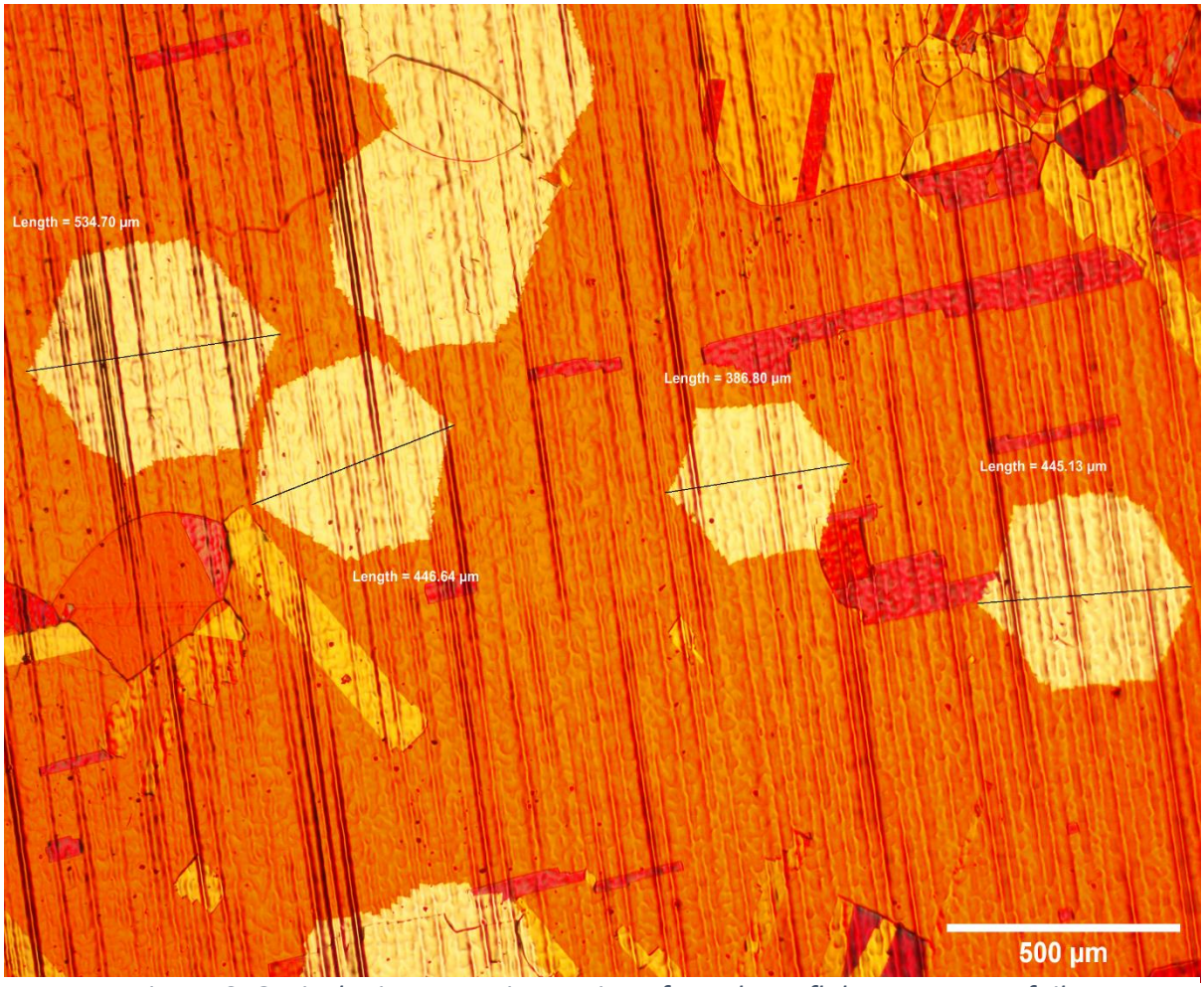

Figure 6: Optical microscope inspection of graphene flakes on copper foil.

Optical inspection of the samples during the microfabrication processes revealed that debris is formed during the ICP oxygen plasma etching of the 2DM material stack (see Figure 4). This is a potential indicator that the reaction of oxygen with the 2DMs is originating solid by-products, such as B_2O_3[12], rather than easily vented gaseous ones.

Atomic force microscope (AFM) was also performed by a collaborator (João Rodrigues) which determined that the hBN thickness ranges from **2 to 4 nm** and that on the border of the samples small nanoscopic silicon oxide particles are being formed due to sublimation of the quartz reaction tube, as shown in Figure 7.

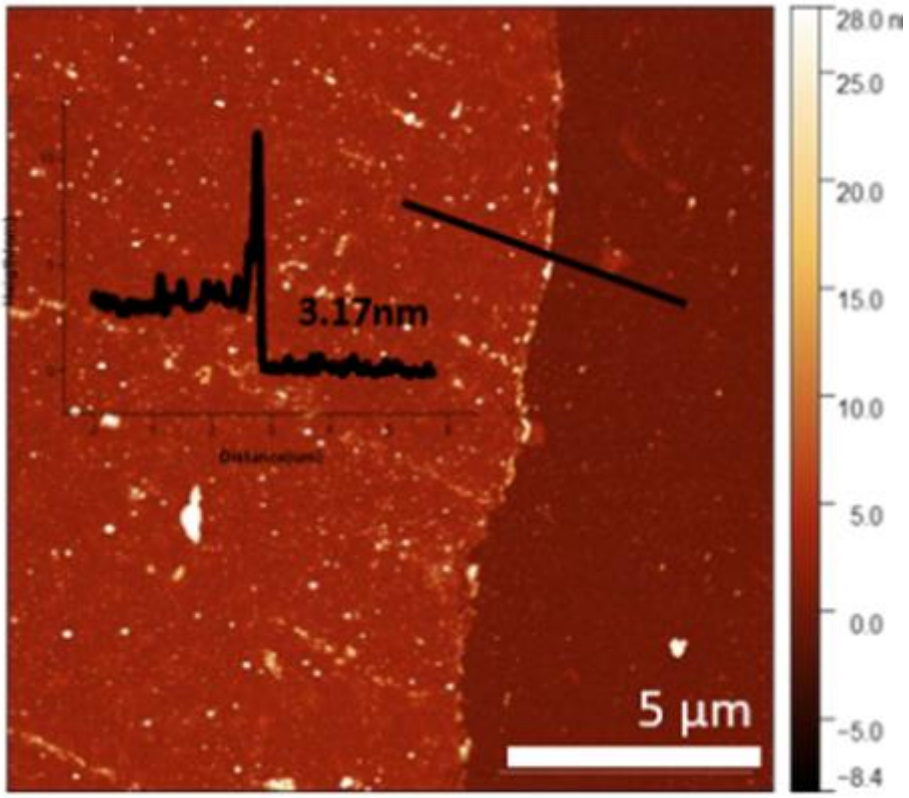

Figure 7: AFM and line scan profile of the hBN film.

In conclusion, a LP-CVD process was successfully optimised for the fabrication of large single crystal graphene flakes and large grain continuous graphene films in relatively short growth time frames (30 min to 2 hours). A potential issue was also identified in the silicate formation in the hBN, which may interfere in the fabrication and optical characterisation of devices.

-WP2.2. Material quality characterisation

Raman spectroscopy was performed using a Witec Alpha 300R confocal microscope Raman system to evaluate the monolayer nature and overall material quality of the CVD grown 2D materials and to check the completeness of the 2D material etching steps during the heterostructure microfabrication processes. Excitation was carried out utilising a Nd:YAG laser of wavelength 532 nm at 2.51 mW power. The signal collection was done using an objective of x50 magnification and 0.7 NA, and the detection was done using a 600 gratings/mm monochromator and UHTS300 spectrometers coupled to the Andor Peltier cooled CCD detectors.

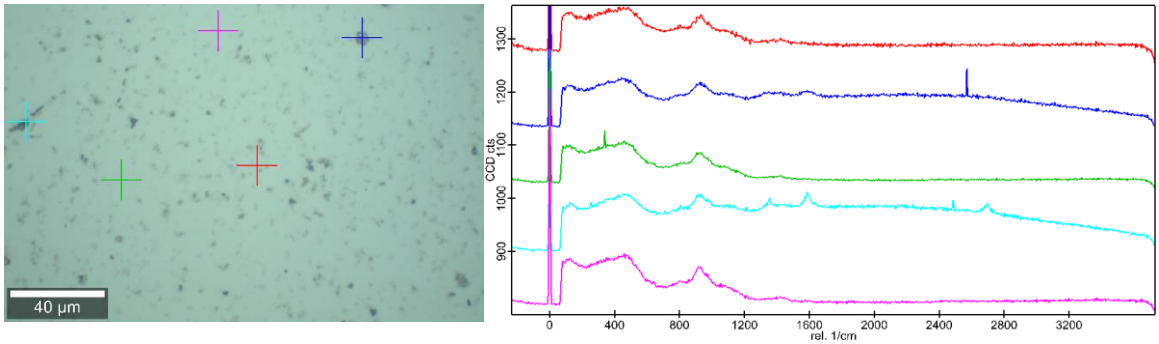

Figure 8: Optical microscope image of the debris produced during the etching of the 2D material stack in the heterostructure microfabrication process (left) and spectra found in the region, colour coded to correspond to the coloured crosses in the optical microscope image. An objective of magnification 50 was utilized.

Figure 8 confirms that, although there is carbon debris remaining on the sample's surface (dark blue and cyan spectra), the oxygen plasma etching process was successful at removing the material for the purposes of patterning the heterostructure.

In conclusion, the oxygen plasma process mentioned in the device processes (WP1.2.2.) is producing carbon debris and, although for the purposes of electrically modulating the graphene's Fermi level this etching technique suffices, it creates visual clutter that may interfere with the optical measurements. The characterisation of material quality was also executed within the intended timeframe (First 8 months).

-WP2.3. Single emitter characterisation using Widefield TIRF Microscopy

A Nikon Ti-E wide-field **total internal reflection fluorescence (TIRF) microscope** was used to localise and probe SPE brightness over prolonged excitation. Excitation of the hBN colour centres was carried out using different excitation wavelengths (488, 561, and 647 nm) and different powers to study how the quantum emitters' behaviour changes in function of these parameters, the fluorescence emissions signals were collected using an oil immersion lens of x60 magnification, and recorded using an Andor IXon Ultra 897 EMCCD camera. This technique was also used to compare CVD grown hBN with liquid phased exfoliated (LPE) hBN.

Widefield TIRF measurements, which consisted of 2 minute long recordings with integration time of 50 ms per frame, were collected on hBN samples in areas of 138.24 by 138.24 μm^2. For 4 of these areas, smaller regions of interest of 34.56 by 34.56 μm^2 were selected within the most focused part of the recordings to ensure that all SPEs in the analysed area are accounted for. Values for the surface density of emitters, intensity time

traces, and statistics for fluorescence intermittency events in hBN were extracted using the image processing methodologies explained in WP3.

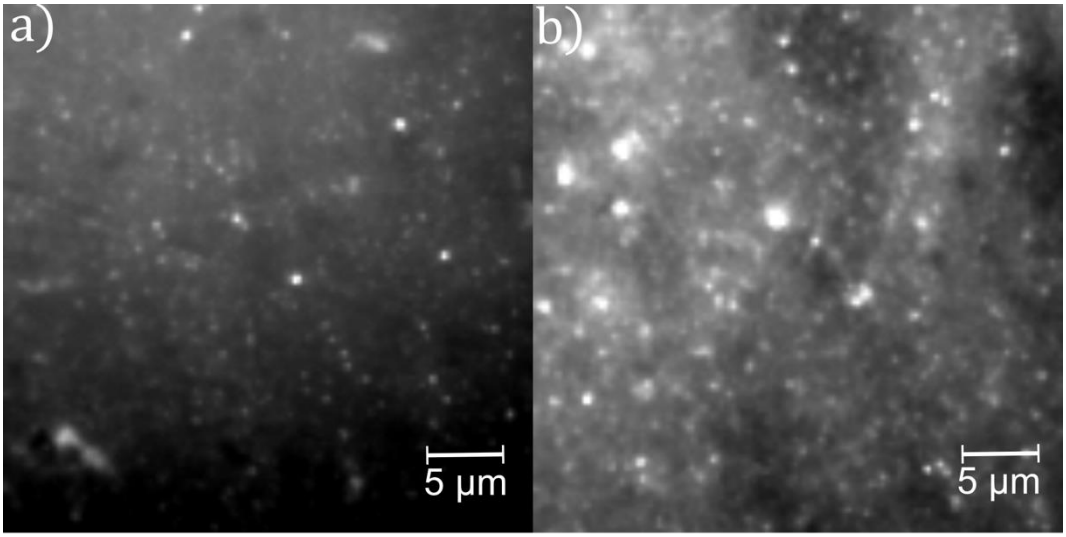

Figure 9: TIRF microscopy images of SPEs in CVD grown hBN (a) and drop cast LPE hBN (b).

In conclusion, single photon emitters were successfully located and their fluorescence signal was recorded using wide-field TIRFM, in accordance to the work plan (First 8 months). Fluorescence intermittency behaviours and data sets with pertinent information on SPE properties were recorded at different excitation conditions.

-WP2.4. Single emitter characterisation using lambda mode confocal fluorescence Microscopy

A Zeiss LSM 780 confocal microscope, equipped with a 32 channel GaAsP detector for spectral imaging was used. An oil immersion objective of NA 1.4 and magnification 63x was used to collect the signal. The spectral detection widow across 32 channels of the detector was set to cover an emission wavelength range from 405 to 696 nm, while only the channels covering the range from 520 to 696 nm were considered for the analysis, due to contamination of the remaining channels with scattered laser light. An argon laser's emission line at 488 nm was used to excite the hBN samples at 12.5 mW average power. The 2048 by 2048 pixel hyperspectral confocal fluorescence images (Figure 10) of 32.72 by 32.72 μm^2 CVD grown and drop castes LPE hBN sample areas are formed by scanning the hBN samples with the laser beam and acquiring the signal pixel by pixel with approximately 50 µs integration time and 16 averages per pixel, resulting in a total acquisition time of 1 hour.

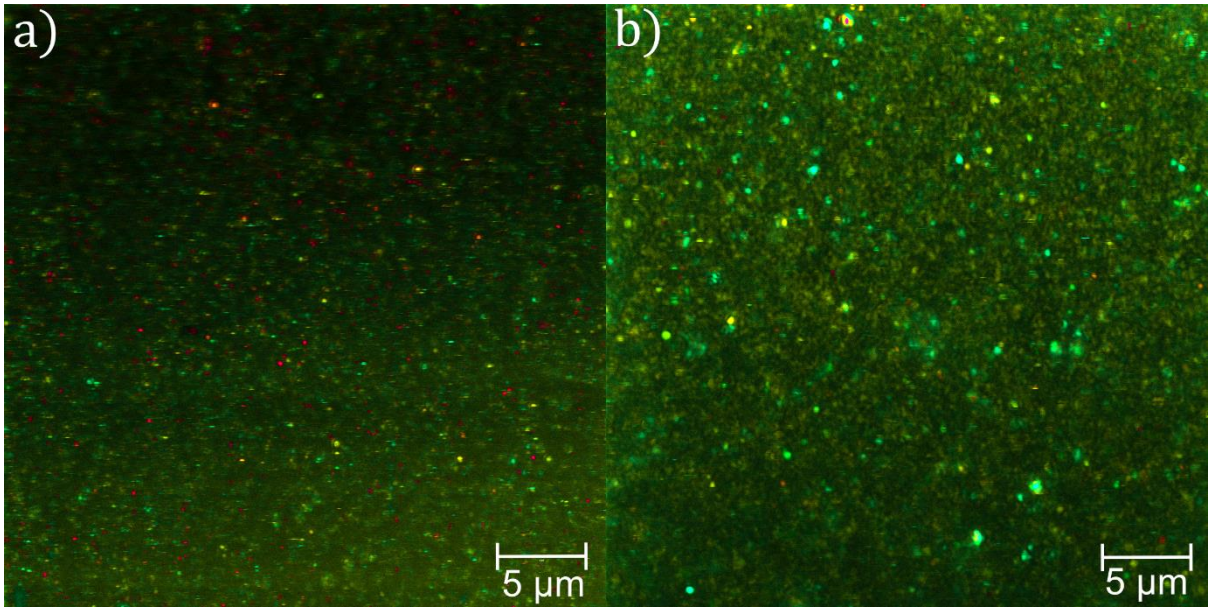

Figure 10: Hyperspectral Fluorescence intensity images of CVD grown (a) and drop casted LPE hBN (b) samples as measured using the Nikon Ti-E wide field TIRF microscope.

In conclusion, very rich data sets containing information on the spectral characteristics of hBN SPEs for two types of hBN sample preparation were gathered, enabling detailed analysis of the emission properties using in-house designed methodologies. This activity was accomplished within the workplan's intended date of the first 12 months of PhD. A potential improvement on this analysis would be to utilise a higher spectral resolution technique.

-WP2.5. Single emitter characterisation using fluorescence lifetime imaging microscopy

Fluorescence lifetime imaging microscopy (FLIM) was used to probe the fluorescence lifetimes of emitters in LPE hBN. The setup, illustrated in Figure 11, uses a pulsed 561 nm wavelength laser whose light is injected into the microscope objective (x100 magnification with 1.45 NA oil immersion lens) though a beam expander. A piezoelectric stage with nanometric precision on top of a micrometric precision stage is used to move the sample and perform point-by-point signal acquisition of sample areas. The signal emitted by the sample is filtered by a bandpass filter (600 ± nm) and a long pass filter (>561 nm) to minimise signal contamination from external stray light. A single photon avalanche photon diode (SPAD) was used to transduce the fluorescent signal into an electric one which is injected into a time correlated single photon counting (TCSPC) card. The synchronisation signal (SYNC), which triggers the photon counting function of

the TCSPC card, is provided by the laser which can function at 20 MHz and at 50 MHz pulse rate.

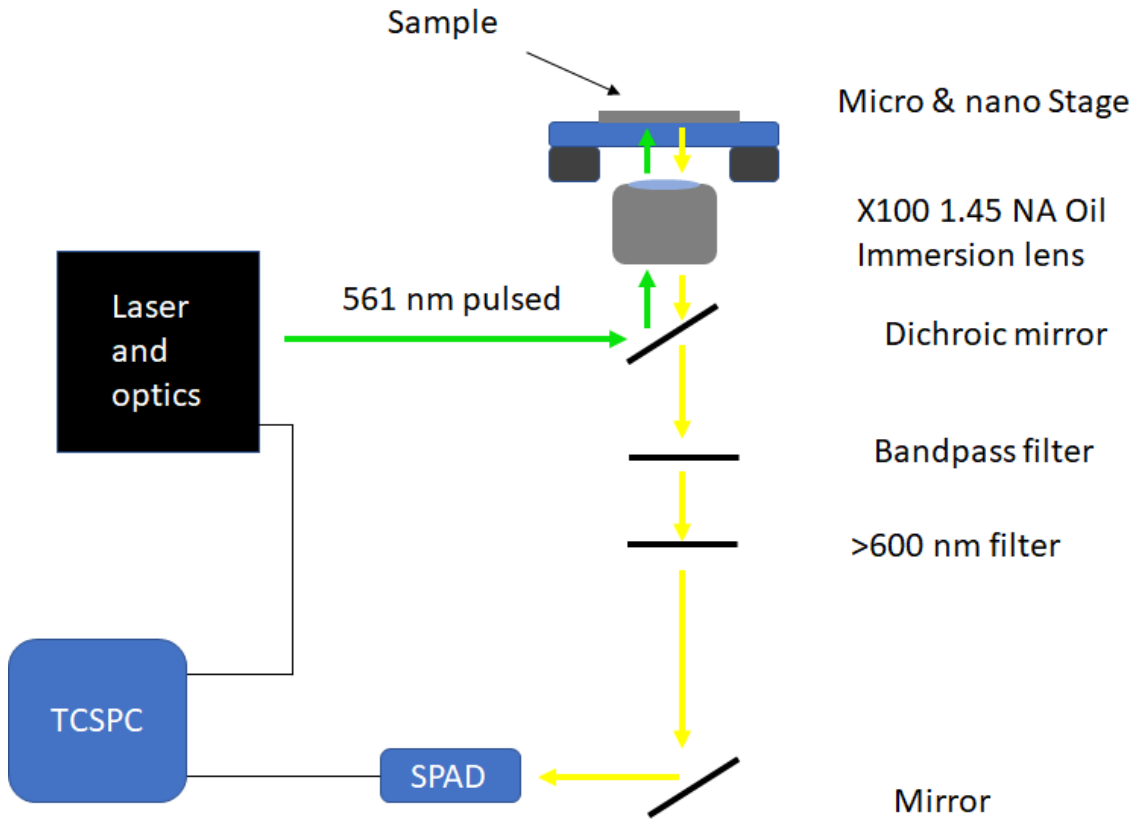

Figure 11: Diagram of the FLIM setup used.

-WP2.6. Single emitter characterisation using the Hanbury-Brown-Twiss experiment

The Hanbury-Brown-Twiss (HBT) experiment is the standard for probing the single photon emitter nature of the fluorescent spots in hBN. It consists in measuring the second order correlation curve ($g^2(\tau)$), which describes the probability of there being a photon arrival at a given detector after a detection having already occurred at another detector a given time before (τ). For a single photon source, in an ideal HBT experiment setup, the value for $g^2(0)$ is 0, which is to say that coincident detection should be impossibleFigure 12. In practice, due to the SPAD detectors having ~37% quantum efficiency, a dead time larger than the SPE's average lifetime, and contamination of the experiment due to stray external light being possible, measured values for $g^2(0)$ are superior to 0, with $g^2(0) < 0.5$ being considered the standard value for what's considered a good SPE light source.

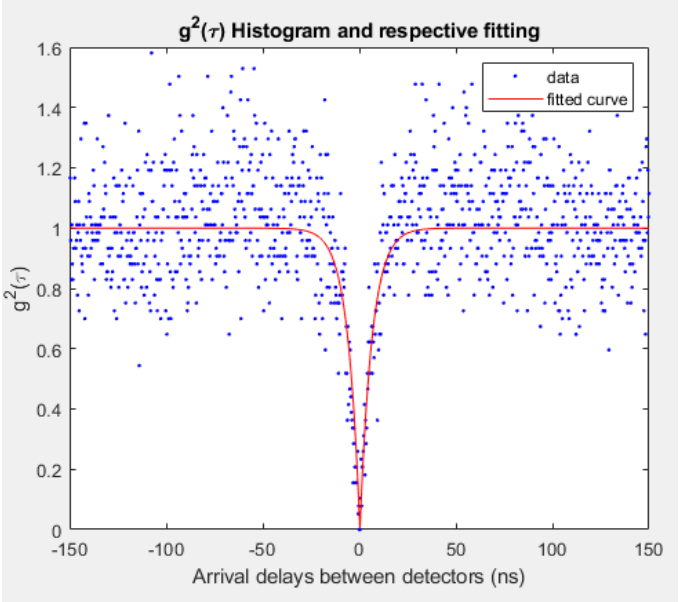

Figure 12: Monte-Carlo simulation of the second order correlation function of an hBN SPE considering ideal experimental setting and SPAD parameters.

It was the first time this experiment was carried out at INL and skills in optical system alignment had to be cultivated to attempt the experiment. A start-stop measurement was implemented, where a photon arrival at detector 1 starts the TCSPC timer and an arrival at detector 2 stops the timer. A histogram is then constructed from the arrival time differences between detectors.

The experiment was tried with two different lasers: a continuous wave 532 nm wavelength laser and a 561 nm pulsed laser. For CW excitation, the expected output is a dip in the shape of a decaying exponential ($\sim e^{-|\tau - t|}$), where t is a delay introduced by the length difference in the optical path of the photons, and potentially delays introduced by differences in cable length between the cables that connect the SPADs to the TCSPC card. For pulsed excitation, the expected output is a sequence of exponentially decaying pulses whose spacing along the time axis depends on the laser pulse frequency and where once of the central peak will have lower amplitude at the same time delay where the dip happens when using CW excitation.

A difference in cable length of 6 m was introduced between the cables that connect each SPAD to the TCSPC card with the purpose of introducing a delay time between the electric pulse arrivals, such that the dip of the auto-correlation curve would appear at $\tau \approx$ 22.2 ns for better visualisation of the full curve.

Band-pass and long-pass filters truncate laser reflections, background fluorescence, and other stray light that may interfere with the measurement.

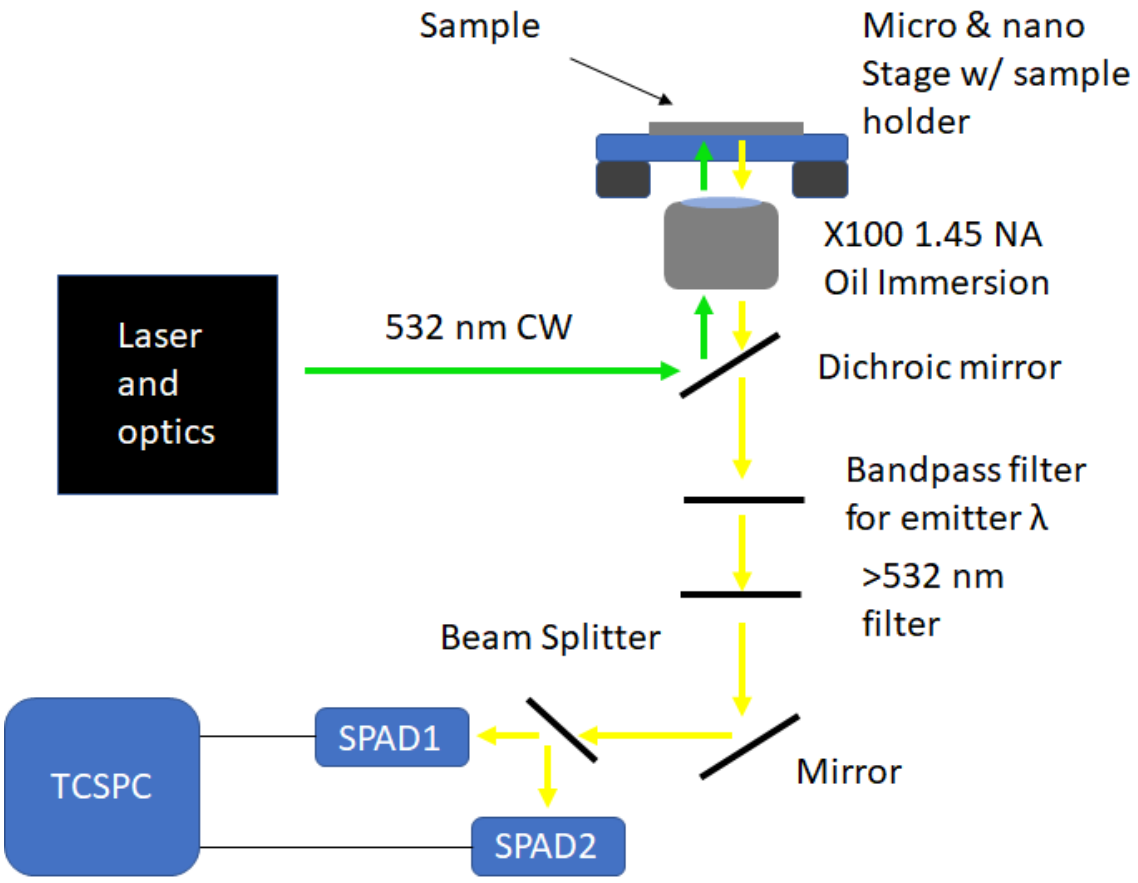

Figure 13: Hanbury-Brown-Twiss experiment setup.

WP3: Development of new methodologies for SPE data analysis

-WP3.1. Protocols for analysis of Widefield TIRF recordings.

For image processing, the ThunderSTORM plugin in ImageJ was used to localise intensity spots of the size of the PSF to extract locations of single-photon emitters across different areas of the samples recorded using the wide-field TIRF setup. From the resulting coordinates table, we filter out the emitters whose standard deviation of detection by the fitting process exceeds 50 nm to ensure that the emitters are being accurately selected. A table of intensity values over time for each detected emitter is

extracted using ImageJ and analysed using custom **MATLAB scripts** that plot the emitters' intensity time trace.

From the careful observation of hBN SPEs' time traces it became apparent that **hBN is a very rich system in terms of fluorescence intermittency behaviours**[13,14], since a total of 4 distinct behaviours were identified (Figure 14). Two of these intermittency behaviours were labelled as high intensity and low intensity photo-stable (**High PS and Low PS**), since they actually displayed no intermittency and only very small intensity fluctuations, but differed in mean intensity value. Another intermittency behaviour as labelled as spiking (**Spikes**), where mostly stable SPEs would occasionally produce very bright spikes in intensity. Lastly, the most noticeable flickering behaviour was labelled as **wavy or step** due to the clear sinus or square wave intensity trace shape that shows clear transitions between dark and bright emitter states.

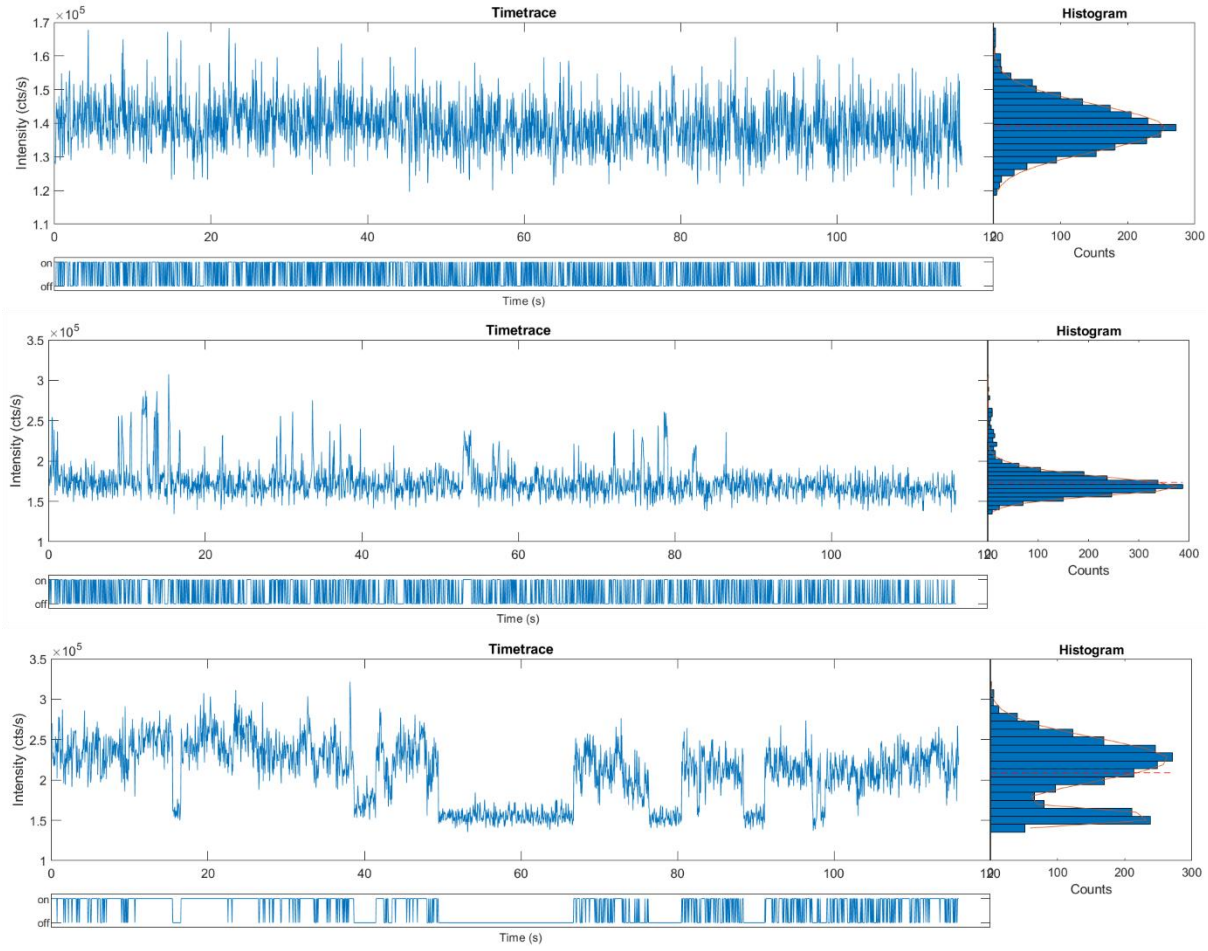

Figure 14: Examples of hBN SPE categories based on fluorescence intermittency behaviour. Low intensity photo-stable (top), Spikes (middle), Wavy or Step (bottom). The intensity distribution histograms and Bright/Dark binary time trace bars are also included.

Several iterations of a custom MATLAB script for the automatic classification of the SPEs according to their intensity time trace were implemented. The final and most reliable version of the script follows the ensuing algorithm:

For each detected emitter, a histogram distribution is made by binning the recorded intensity values in accordance to Scott's law. To determine a threshold value which separates the dark and bright states' intensities, a weighted average is performed using the histogram distribution, such that the bin values with a larger number of counts are favoured. Because the distribution of intensities follows either a Gaussian pattern or a sum of two Gaussian patterns, when the Bright and Dark states are more easily distinguishable, the weighted average results in either a threshold very central to the Gaussian distribution or a value in between both Gaussians (See histograms in Figure 14). The threshold value, th, is then determined by the expression:

$$\mathrm{th} = \sum_{\mathrm{i}} \frac{\mathrm{histo(i)}}{\mathrm{sum(histo)}} . \mathrm{histbin(i)}$$

Where $histo(i)$ is the number of intensity values in the i-th bucket, $histbin(i)$ is the central intensity value associated with the i-th bucket, and $sum(histo)$ is the total number of recorded intensity values for a give trace.

A binary time trace of Bright and Dark states can now be determined by thresholding the intensity time trace. The following step is to count the time duration of the Bright and Dark state time intervals using the binary time trace. It was clear that the **variance of these time duration values was a good distinguishing factor between photo-stable and intermittent emitters**, since intensity fluctuations in stable emitters are always in the order of up to a few tens of ms and in wavy or step type of emitters they can range from tens of milliseconds to tens of seconds, thus have substantially higher time duration variance.

Using the Bright and Dark state time duration variance, an intensity amplitude limit, and the overall mean intensity over time, the categorisation of the SPEs follows these rules: If the time duration variance of the Dark and Bright states exceeds 0.01 then the emitter belongs to the Wavy or Step category, otherwise if the emitter intensity exceeds 1.4 times the mean intensity value or is below 0.6 times the mean intensity value then the emitter belongs in the spikes category, since it is too stable to accuse flickering but still possesses a large intensity amplitude. Lastly, in the event that the previous conditions fail, if the emitter mean intensity surpasses the mean intensity of all emitters in the sample then it belongs in the high intensity photo-stable category, otherwise it belongs in the low intensity photo-stable category.

This algorithm enable the counting of SPEs in a sample per flickering behaviour category, and also the **estimation of emitter density under different excitation parameters.**

In conclusion, image processing tools were optimised to locate SPEs in TIRFM data sets and custom MATLAB scripts were developed to extract useful information to analyse, such as emitter intensity over time. Four categories of hBN SPE behaviour were identified based on fluorescence intermittency and brightness and statistical analysis of the

identified SPEs was carried out in function of excitation wavelength and power. This too was accomplished within its intended time frame, within the first 12 months.

-WP3.2. Protocols for spectral analysis and extraction of useful data from confocal fluorescence microscopy hyperspectral data sets.

To analyse the data obtained via the confocal fluorescence microscope, the **Zeiss Zen Black 3.0** software was used to extract the signature spectra of hBN SPEs and to perform linear unmixing of the recorded images, breaking down the data into 3 intensity maps associated to SPE spectra found in the samples.

Because the hyperspectral images are formed by scanning the sample from left to right and top to bottom, SPEs that display **fluorescence intermittence behaviours** are displayed in the measurement as dashes, half-circles, or interrupted circles, due to the imaging of the pixels of a given SPE being done non-sequentially, such that there are timeframes where when the emitter is being scanned it is in a dark state. ImageJ was used to segment the linear unmixed channels into SPEs and background via thresholding, and to perform the emitter counting by using the built in automatic particle counting tool, which results in the extraction of a data table containing coordinates and shape descriptor values which can be used to classify SPEs as blinkers and non-blinkers.

Using MATLAB's curve fitting toolbox, Gaussian fits of the SPEs' intensity profiles were performed and compared to the expected point spread function (PSF) of a point source of light as observed by the Zeiss LSM 780 confocal microscope.

Detailed analysis of the unmixed data was also carried out for selected SPEs to confirm **spectral diffusion behaviours**[15,16] by using custom MATLAB scripts. The same area from the centre of the same SPE's PSF was selected in linear unmixed intensity maps corresponding to different spectra and, since pixel dwell is the same for all pixels during the measurement, a timestamp was attributed to each pixel such that a pseudo-time intensity trace corresponding to one each of the spectra could be plotted. Comparing the pseudo-time traces for anti-correlations can reveal the spectral diffusion behaviour.

In conclusion, custom MATLAB scripts in conjunction with ImageJ and Zeiss Zen 3.0 were used to perform image processing on hyperspectral data sets acquired by laser scanning confocal fluorescence microscopy to perform a detailed study of the optical

properties of hBN SPEs, such as emission spectra, fluorescence intermittency, and spectral diffusion. The time frame for the task's completion was within the first 12 months and it was met.

Results

-Graphene properties

A myriad of parameters was tested in graphene CVD and their respective effects were analysed and noted. It was observed that morphology varied from sharp edged "star" shapes to circular graphene blobs, and recipe optimisation enabled expansion of flake size from approximately **200 µm to over 1500 µm in diameter**. Recipes were also successfully adapted for continuous graphene film fabrication by adjusting the growth time.

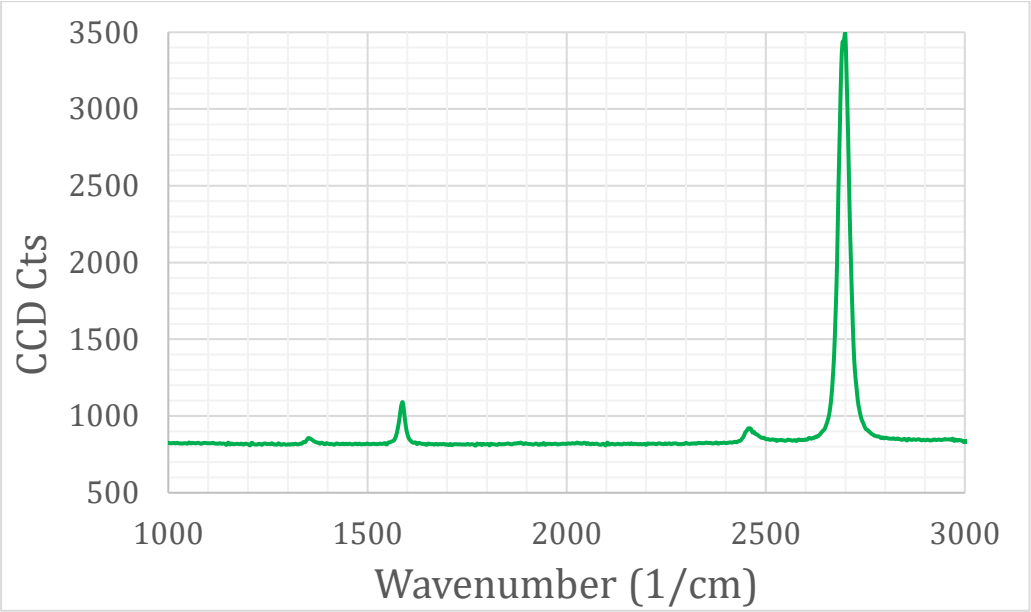

Figure 15: Raman spectrum of a continuous graphene film. Excitation as done using a 532 nm wavelength Nd:YAG laser at 2.51 mW power. Signal was acquired with a 5 s integration time and was averaged 10 times.

Analysing the Raman spectrum for graphene in Figure 15 it is clear that the material is monolayer since the 2D peak (~2699.9 cm^{-1}), which is characteristic of monolayer graphene, is far larger than twice the G peak (1588.5 cm^{-1}), which is the signature for graphitic materials. Furthermore, the comparatively minuscule D peak

(1351.7 cm^{-1}), which pertains to defects in the graphene's crystal lattice, indicates that the material has **excellent crystallinity**[17].

-Density of defects in hBN

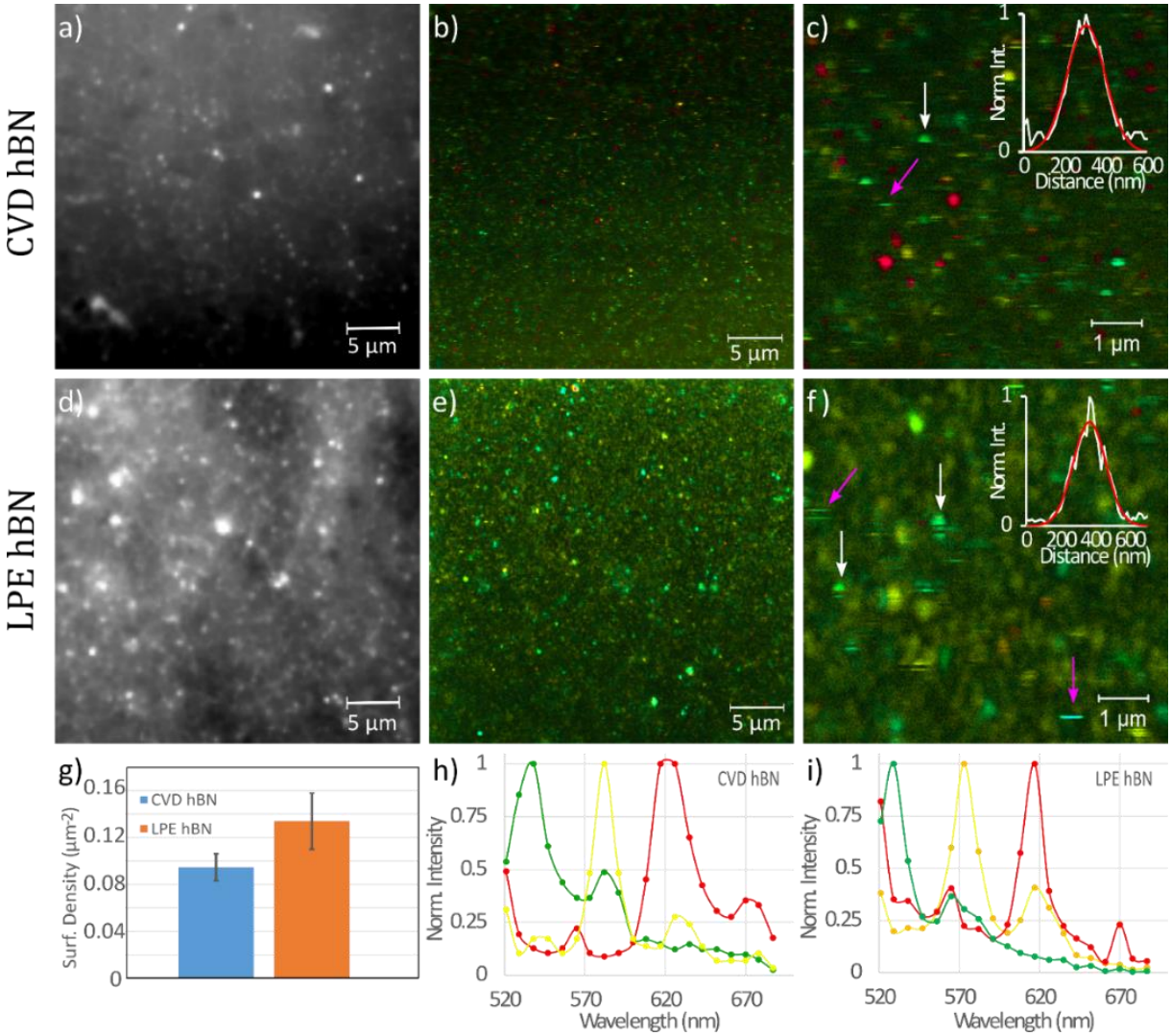

Figure 16: Fluorescence intensity and spectral analysis of the two hBN samples. Panels a), b), and c) pertain CVD hBN, as follows: (a) fluorescence intensity image as observed by TIRFM, (b) hyperspectral confocal fluorescence image (the colors correlate to the recorded spectral components at each pixel), (c) zoomed-in confocal fluorescent image with inset illustrating the intensity profile of one fluorescent spot and its Gaussian fitting. Panels d), e), and f) represent the same information for LPE hBN. In the confocal images (over 33.7x33.7 µm² areas), the density appeared as 0.68±0.15 and 0.23±0.05 emitters/µm2, respectively. The difference with the TIRF measurements is related to a lower counting accuracy in the confocal microscopy data, due to noise artefacts in the automatic counting algorithm (see section 2.4.8). Panel g) represents the mean emitter surface density values extracted for both samples using the TIRFM system. Panels h) and i) reveal the most representative spectra observed in each sample.

Single photon emitter (SPE) signatures can be observed in confocal fluorescence intensity images (Figure 16 b, c, e , and f). The intensity spot shapes largely match the point spread function (PSF) of the microscope (see Figure insets). The PSF for a 488 nm laser and a microscope objective of magnification 63x used with an NA of 1.4 is 220.4 nm and the order of magnitude was verified by performing Gaussian fittings to the intensity profiles, resulting in widths of 217.8 nm and 222.5 nm for CVD and drop cast liquid phase exfoliated (LPE) hBN material, respectively.

We analysed the single emitter density by determining the **number of SPEs visible in CVD grown and exfoliated hBN samples per unit area**. In the confocal image scans performed over areas of 33.72 by 33.72 μm^2 the density is **$0.675 \pm 0.153\ \mu m^{-2}$** and **$0.230 \pm 0.047\ \mu m^{-2}$** for CVD and DC samples, respectively. Additionally, a faster imaging technique was used to inspect the samples, which may results in slightly different numbers per area due to less integration time per image and thus less laser power/ bleaching effects. From images recorded in shorter time (50 ms versus 61 minutes) on this wide-field TIRFM system (Figure 16 a and d) we extract that both the AP-CVD prepared hBN sample and the drop cast LPE hBN sample have similar emitter densities of **$0.095 \pm 0.012\ \mu m^{-2}$** and **$0.134 \pm 0.024\ \mu m^{-2}$,** respectively, which correspond to mean distances between emitters of 3.25 ± 0.21 μm for the CVD grown hBN sample and of 2.73 ± 0.27 μm for the LPE hBN sample.

Reported SPE surface density in CVD grown samples varies significantly, with some groups reporting densities as low as 0.04 emitters/μm^2 [13] to higher values such as 2.2 emitters/ μm^2 [18]. In contrast, our CVD grown hBN stands in between with a density of 0.095 ± 0.012 emitters/ μm^2, which we believe can be an **advantageous characteristic**[19] in terms of making our hBN a good host material for producing large amounts of devices per unit area whilst lessening the difficulty of ensuring that only isolated emitters are used in device fabrication.

-Advanced hBN SPE spectra characteristics and intermittency behaviour

Fluorescence confocal microscopy allowed us identify different emitter types that can be excited with a 488 nm laser either via the excitation of the electronic transition or via absorption in higher lying e.g. vibrational bands, resulting in large stokes shifts, and emission peak maxima positions positioned as far apart from the excitation wavelength at **538 , 582, and 617 nm** for the representative emission spectra observed for emitters in AP- CVD grown samples (see Figure 17 a) the green , yellow and red spectra , and at **538 , 571, and 617 nm** for the representative emission spectra observed for emitters in drop cast LPE samples (Figure 17 b), respectively.

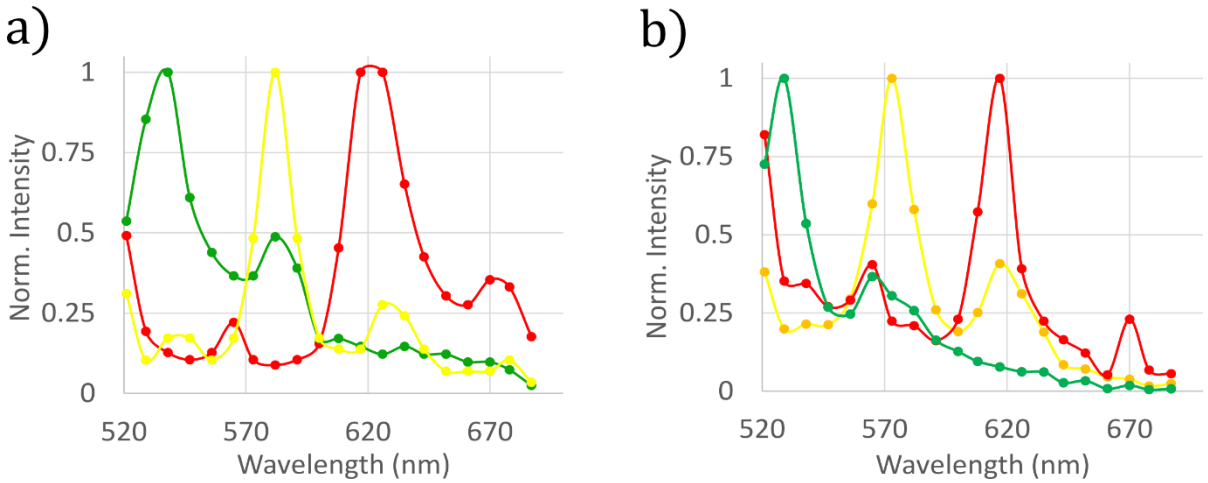

Figure 17: Spectral components isolated from the fluorescence confocal microscopy measurements. Image a) refers to the components selected in the CVD grown hBN sample and b) to the drop casted PLE hBN sample.

The energy differences between the associated high intensity emission peaks and the lower energy peak apparent as a red shifted shoulder, have been determined to be 0.175 eV , 0.150 eV and 0.159 eV for AP-CVD recoded spectra with emission peak maxima at 538 , 582, and 617 nm and to be separated by 0.150 eV, 0.155 eV , 0.159 eV and 0.159 eV in case of exfoliated hBN samples for spectra recorded with emission peak maxima at 529 nm , 571 nm and 617 nm, respectively. IN wavelength this shift is on average $\Delta\lambda = 45.7 \pm 6.5$ nm.

The data recorded on the confocal microscope contains further spectral information. Through the analysis of the spectral fingerprints, of which there are several as seen in literature[20,21], associated to the pixels of the image we **performed a linear spectral unmixing** of the data set using 3 spectral categories for each of the CVD and exfoliated samples, respectively (Figure 17). The colour of the images (Figure 18 a and c)

reflects the spectral composition of the fluorescence emission detected across the CVD and DC samples, with additive spectral colour mixture across the detection range (520 to 696 nm).

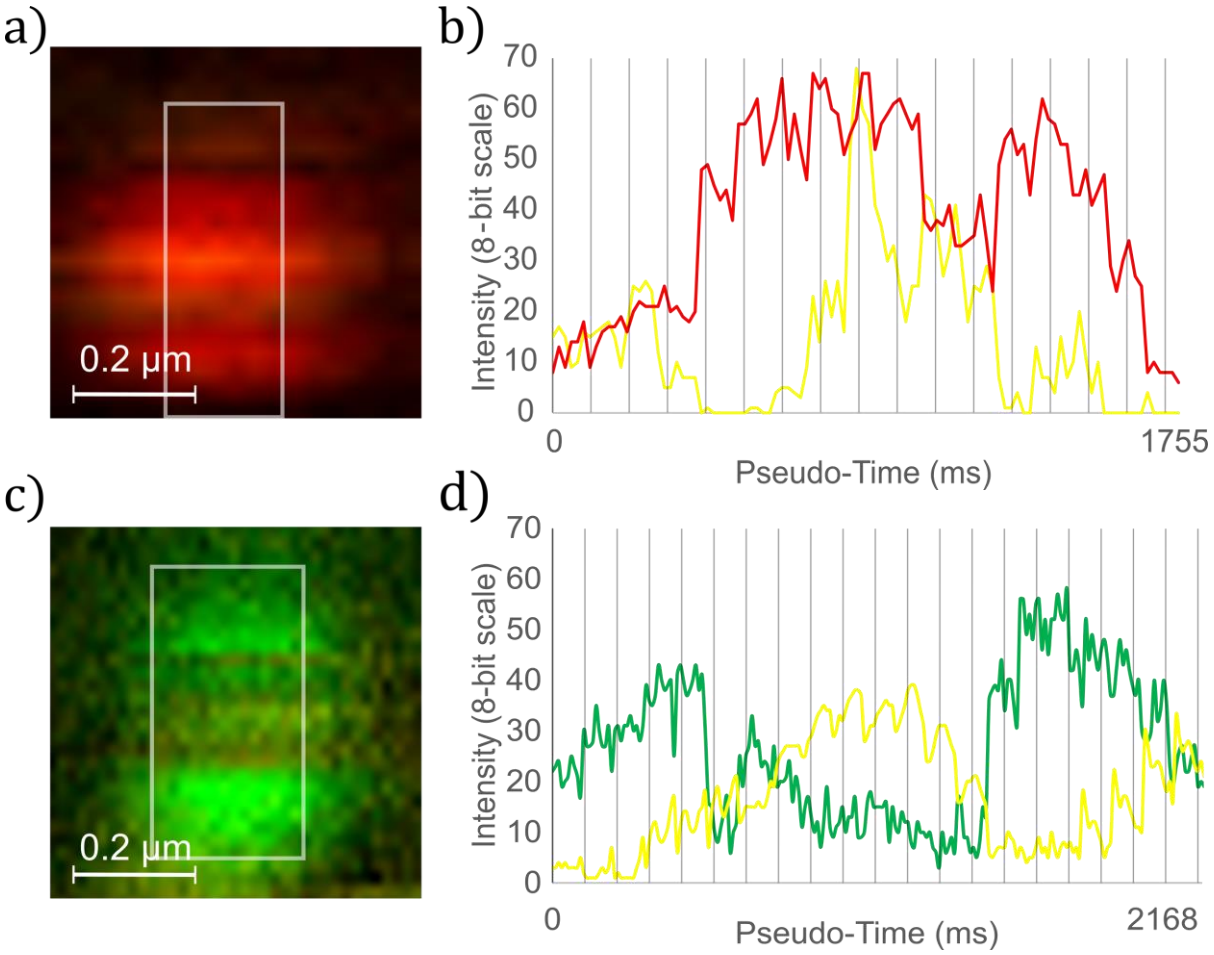

Figure 18: Observations of PSF confined fluorescent spots in hBN displaying large spectral changes. a) Fluorescent spot present in CVD hBN undergoing spectral changes mid-measurement and area analysed to extract intensity of fixed spectral components over time; b) Overlap time traces of the spectral components for 617 nm and 571 nm contained in the spot (a); c) and d) are equivalent to a) and b) but for another fluorescent spot, this time present in an LPE hBN sample, and for spectral components 571 nm and 538 nm.

At some few positions in the image intensity spots with different emission spectra are located in the same area of the PSF, either caused by two defects so close that they are not spatially distinguished with the confocal diffraction limited spatial resolution of the microscope or if both 'colours' blink at the same time - it would indicate that **a single centre would be able to undergo large spectral changes in time,** as indicated by the anti-correlation revealed in the pseudo-time trace between two spectral components of the drop cast, an effect that has been previously observed. The pseudo-time trace of

component 1 represented as the green curve in Figure 18 (d) refers to the spectral component of maximum of emission at wavelength of 538 nm, and the pseudo-time trace of component 2 refers to the component of maximum of emission at wavelength of 571 nm is represented by the yellow curve in the same figure.

Intermittent blinking processes manifest themselves as deviations from circular intensity spot patterns in the fluorescence intensity images recorded by laser scanning confocal imaging, which was performed from the top to the bottom and from left to right across the characterised sample area.

The blinking associated deviations from circular shapes include, intensity spots in the shape of half circles (highlighted by white arrows), single lines or stripes (highlighted by magenta arrows).

Analysis of SPE statistics based on their spectra revealed that 28.42% of the SPEs in our AP-CVD hBN have a 538 nm intensity peak maximum signature, 25.82% have their peak intensity at 591 nm, and 47.76% have their maximum at 617 nm, whereas in the drop cast LPE sample these statistics are 36.05%, 42.29%, and 21.66% for spectral signatures with emission peak maxima at 529 nm, 565 nm and 617 nm, respectively. Spot shape analysis also enabled the extraction of SPE statistics based on fluorescence intermittency behaviour, which indicate that for the AP-CVD hBN 18.67% and 81.33% of emitters are, respectively, non-intermittent and intermittent, and likewise for the LPE hBN 26.86% and 73.14% of emitters are, respectively, non-intermittent and intermittent.

An intensive study of TIRF data gathered on AP-CVD hBN SPEs yielded the following results for the different categories established at different wavelengths and powers of excitation. For the **high intensity photo-stable emitters** it became apparent that for higher excitation power the density of this calls of emitter rises, indicating that higher excitation power may be a requirement for stable non-intermittent emission. It is also noticeable that this category of SPE is more responsive to the 488, and 561 nm excitation than to the 647 nm excitation (Figure 19).

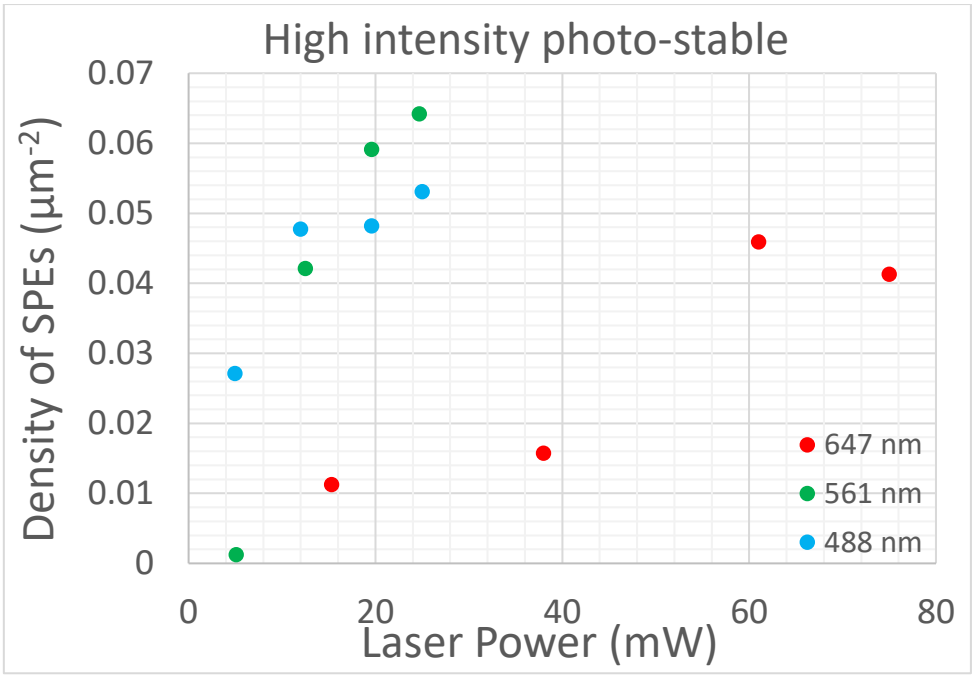

Figure 19: Surface density of high intensity photo-stable SPEs in AP-CVD hBN as determined by the analysis of data sets acquired in the TIRFM setup for different excitation laser powers and wavelengths.

The same behavioural trends as in the **low intensity photo-stable** emitters were observed for their low intensity counterparts, as seen in Figure 20.

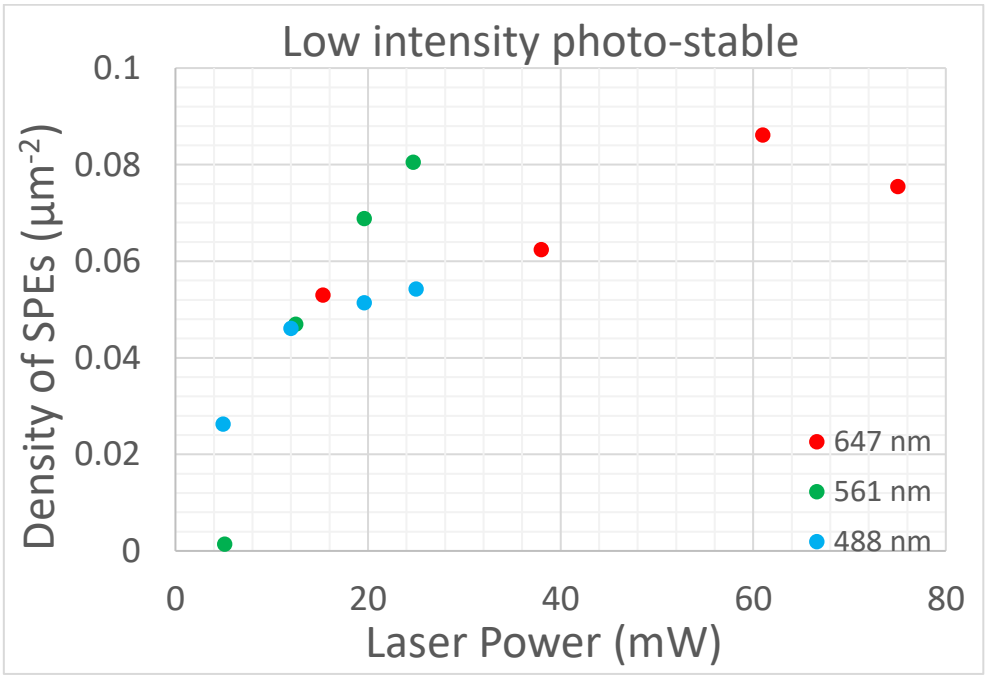

Figure 20: Surface density of low intensity photo-stable SPEs in AP-CVD hBN as determined by the analysis of data sets acquired in the TIRFM setup for different excitation laser powers and wavelengths.

In contrast, the **spikes** category of blinker shows the opposite trend to the stable emitter (Figure 21), where the density of this class decreases to near vanishing degrees with increasing excitation power. It is also notable how this type of emitter is barely activated under 488 nm excitation.

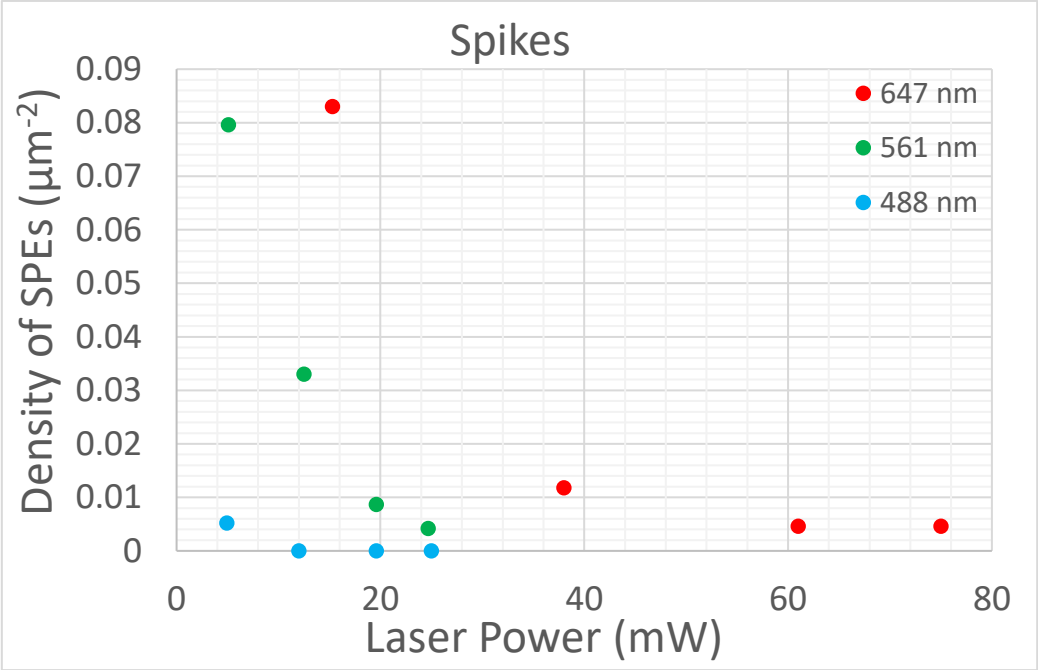

Figure 21: Surface density of spiking SPEs in AP-CVD hBN as determined by the analysis of data sets acquired in the TIRFM setup for different excitation laser powers and wavelengths.

Finally, it was observed that the fluorescence intermittent **wavy or step** category of SPEs were substantially more responsive to 647 nm excitation, and fluctuated with power (Figure 22). The low surface density of intermittent SPEs at 488 nm excitation contrasts heavily with the findings from the analysis of the confocal fluorescence microscope data sets, but since those measurements happen at longer integration times and the signal acquisition is performed pixel per pixel instead of simultaneous image acquisition, as is the case for the TIRFM, we find these results to be more trustworthy.

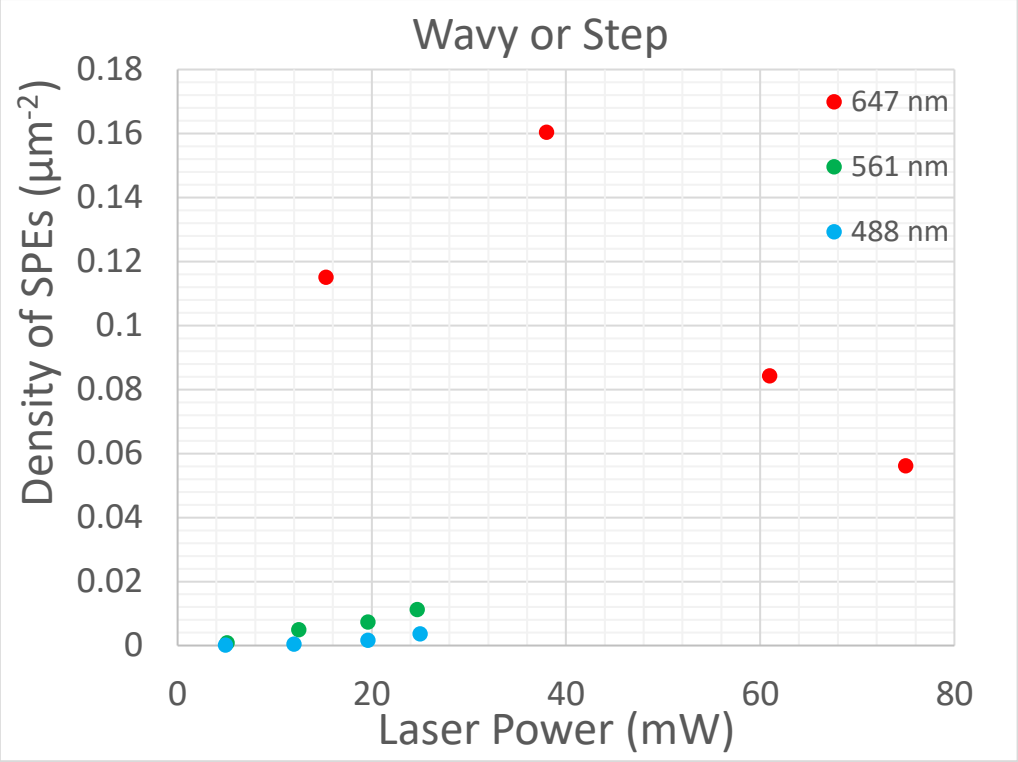

Figure 22: Surface density of wavy or step intermittent SPEs in AP-CVD hBN as determined by the analysis of data sets acquired in the TIRFM setup for different excitation laser powers and wavelengths.

It is also important to note that the duration of the bright and dark time intervals from the wavy or step like intermittent emitters follow a power law statistical distribution as seen in Figure 23, lending credence that the observations are being carried out on single photon emitters. This distribution was obtained by analysing 280 intermittent emitters in CVD hBN under 25 mW 488 nm laser excitation. These statistics are expected for not just hBN[13,22], but also other single photon emitters such as Quantum dots[23] and single molecules[24].

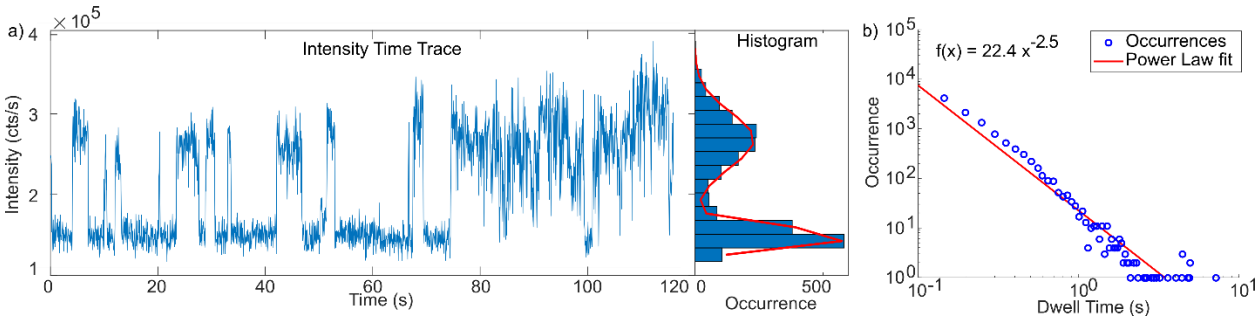

Figure 23: Fluorescence intermittency behaviour of point defects in hBN. a) Fluorescence intensity time trace. The histogram fitted with a double Gaussian curve in red shows the distribution of intensity values across the whole trace revealing a clear distinction between bright and dark states. b) Distribution of the duration times of the bright state for all intermittent emitters recorded. The distribution was fitted to a power law curve whose parameters are displayed in the function f in the inset.

Comparisons of intermittent emitter densities were drawn between AP-CVD hBN and graphene covered AP-CVD hBN to inspect **the effect the presence of graphene** has on the emission characteristics of SPEs.

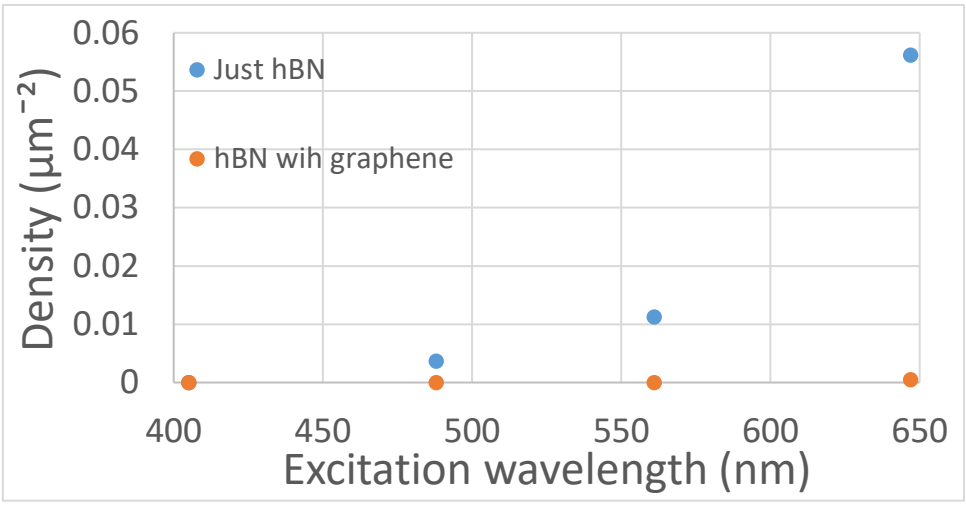

Figure 24: Surface density of fluorescence intermittent wavy or step SPEs in hBN and graphene covered hBN at different wavelengths of excitation at the maximum available powers.

As seen in Figure 24, the addition of graphene to the system produces a passivation effect on the SPEs, resulting in **near total extinguishing of the flickering behaviour**. We attribute this to the redistribution of charge provided by the addition of a metal like layer such as graphene, since the SPEs are environmentally sensitive, this result indicates

that the fluorescence intermittency is mediated by local charge fluctuations in the vicinity of the crystal defects.

-Fluorescence lifetime measurements

The emitters with emission cantered at the 617 nm wavelength were target due to the available excitation wavelengths of 561 nm. A collection time of 2 s was used to collect single lifetime curves and a collection time of 0.1 s was used to image an intensity map of the analysed area in the sample (Figure 25). Bright pixels in the intensity map were selected to acquire fluorescence lifetime histograms.

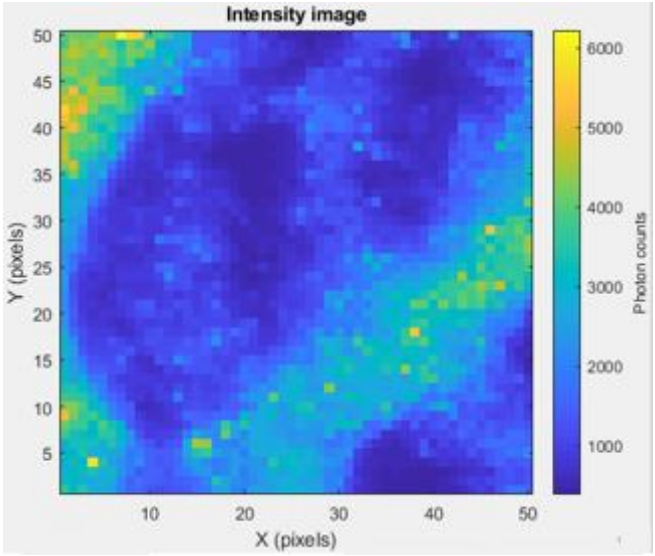

Figure 25: Intensity map in photon counts of an LPE hBN sample. A step size of 50 nm/ pixel was used, such that the scanned area was of 50 x 50 µm2.

The average lifetime was varied, however, a distinction between 2 groups could be made. One group of bright pixels had an average emitter lifetime of 3.06 ± 1.09 ns, which falls well within the values expected when consulting the literature[25,26], whilst the other group was found to have an average lifetime of 1.35 ± 0.34 ns.

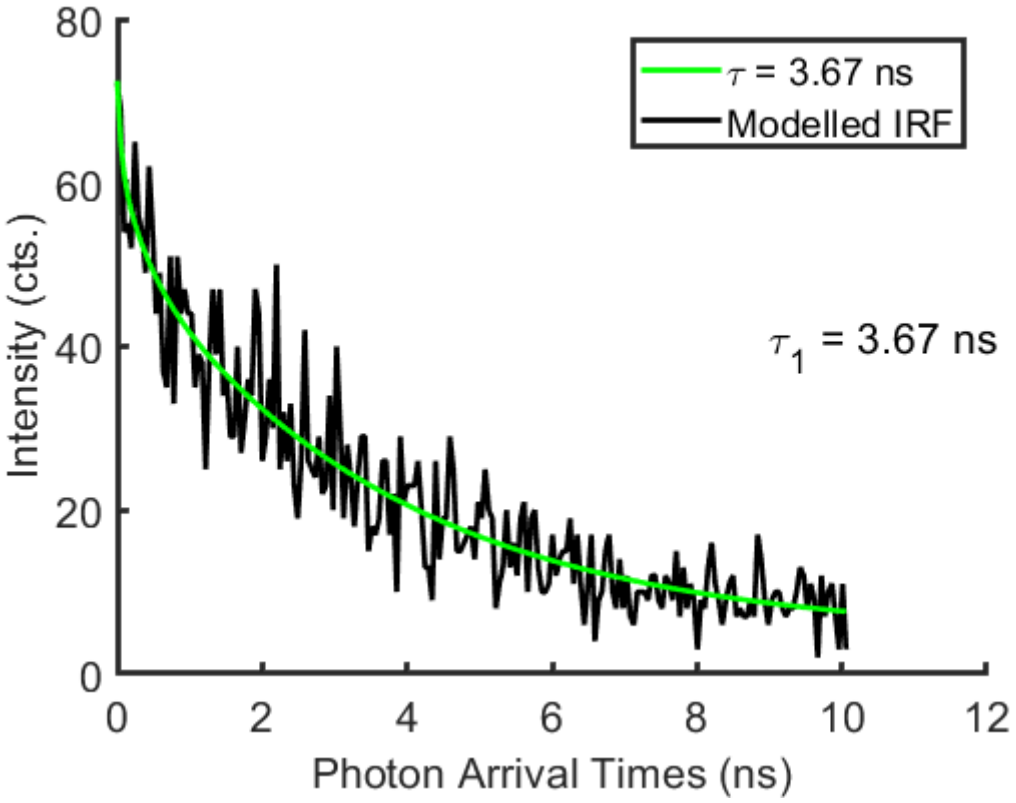

Figure 26: Fluorescence lifetime histogram and exponential fit used to extract the average lifetime from data extracted from the FLIM image (collection time 0.1 s).

-HBT measurements

Several adjustments were done between runs of the experiment. From adjusting the accumulation time (10 min, 30 min, 1 h, 2 h, 8 h, etc…), to changing the detector cable length difference (± 0.5 m, ± 1 m, and ± 2 m), to reducing the excitation laser power in steps using an optical attenuator. Despite these adjustments we continuously got the results indicated in (). When switching the hBN sample by a sample of fluorescent beads we continued to observe the sample outputs, despite expecting a super-poissonian statistics $g^2(\tau)$ signature which consists of an enhanced peak at $\tau = t_{delay}$.

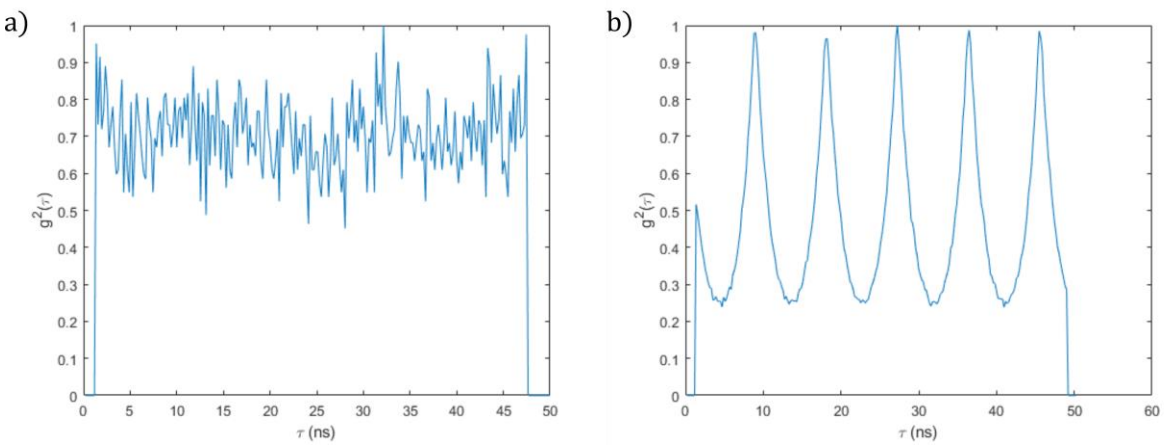

Figure 27: Representative results of the first attempts at performing the HBT sample on hBN SPEs and fluorescent beads. The photon arrival delays were counted during an interval of 1 h and the resulting histogram was normalised. a) Second order correlation curve obtained using CW 532 nm excitation; b) Second order correlation curve obtained using pulsed 561 nm excitation.

Thus, these results suggest that in spite of our attempts to minimise contamination of the experiment with laser reflections and external light, the laser light is still dominating the measured statistics. We intend to overcome this short-coming by replacing SPAD with fiber-couples detectors with higher efficiency and additional light filtering in a future.

Conclusions:

I completed the curricular component of the MAPfis physics doctoral programme, gaining knowledge foundations in the advanced physics topics of nano-optics, advanced material preparation and characterisation, single-photon sources in photonic devices for quantum technologies, and physics of electronics materials and devices;

Four strategies for early prototyping of the Ph.D.'s target device were attempted and allowed for valuable information for the implementation of future designs to be obtained, namely in the fabrication of a largely transparent electric device for modulation of graphene's Fermi level through the application of electrostatic fields. This task is expected to be completed within the first quarter of 2022.

Most planned deliverables, as was the case for reports on material characterisation and on hBN SPE surface density, were met, except for the Hanburry-Brown-Twiss experiment for the confirmation of the quantum mechanical nature of the hBN single-photon emitter, as part of WP3 (to de done within the first half of 2022). Additional work parallel to the scope of the Ph.D. was done, such as LPE hBN characterisation and detailed study statistical analysis of hBN SPEs' fluorescence intermittency behavior.

Large graphene flakes and graphene films of excellent crystallinity were successfully fabricated and characterised, and methods for 2-4 nm hBN CVD growth containing SPE densities of $\mathbf{0.095 \pm 0.012\ \mu m^{-2}}$ were also developed. Additionally, LPE hBN samples were prepared by drop-casting, analysed, and compared to the hBN CVD samples.

The SPE signatures were obtained via confocal fluorescence microscopy and labelled according to their emission peak maxima of **538, 582, and 617 nm** for the CVD hBN sample and **538, 571, and 617 nm** for the LPE drop cast hBN sample. We also observed several replica peaks, typically called phonon sidebands (PSBs), whose wavelength difference from their respective ZPL is $\mathbf{\Delta\lambda = 45.7 \pm 6.5\ nm}$, in agreement with the literature [18,20,27] strengthens that claim that the observed fluorescent spots are SPEs. Significant spectral changes were also observed in some selected SPEs, and an anti-correlation between linear unmixed intensity maps associated with different spectra was analysed to verify this spectral diffusion behaviour.

Statistical analysis of SPEs based on fluorescence intermittency behaviour, of which 4 categories of SPE were identified, was carried out for both TIRFM and confocal fluorescence microscopy data sets, and, in specific for the TIRFM datasets, the effects of excitation power and wavelength on these statistics were studied. This study revealed that SPEs tend to have large densities of stable emitters for higher excitation power across all considered wavelengths and that the high-intensity photo-stable emitters are most responsive to 561 nm excitation wavelength. With increasing power, the spiking behaviour decreases to near vanishing degrees and is exceptionally uncommon under 488 nm excitation. Finally, the wavy or step SPEs are most common under 647 nm excitation.

Characterisation of the fluorescence lifetime of SPEs in hBN was performed and matched the values expected from the already existing literature. Attempts at characterising the single photon emission were carried out via the HBT experiment and, despite adjusting many parameters, we were unable to observe the expected second order correlation curve. Improvements will be made to successfully carry out the experiment in the first half of 2022.

To check how the graphene affects the hBN quantum emitters, TIRFM data sets of graphene covered hBN samples were analysed and the resulting statistics were compared to the statistics of AP-CVD hBN, revealing that the graphene addition results in an almost complete extinguishing of the fluorescence behaviour, most likely due to a passivation effect of local accumulated electric charges in the vicinity of the flickering SPEs, who are environment sensitive[28].

Collaborations

Several collaborations were established to accomplish the reported work and contribute to other work related to the scope of the PhD. The main collaborations were the following:

-Dr. Andrea Capasso (INL), who provided a dispersion of LPE hBN in IPA for the drop cast comparisons;

-João Freitas (INL and U. Minho), received support in data analysis of TIRFM data sets about the study of DNA hybridisation kinetics on the single-molecule level using graphene near-field effects;

-João Rodrigues (INL), performed AFM measurements of AP-CVD hBN samples;

-João Fernandes (U. Minho and INL), provided some AP-CVD hBN samples;

-Prof. Axel Lorke (U. Duisburg Essen), who agreed to host the student at U. Duisburg Essen for cryogenic temperature measurements of hBN SPE spectral properties;

- Graphene RF devices group (U. Bristol), who agree to support the student in the fabrication of active electric matrices for the electrical addressing of many nanoscopic 2D material heterostructures;

-Dr. Jérôme Borme (INL), who gave advice and consultation on the organisation and drafting of the microfabrication process flows;

-Prof. Ricardo Ribeiro (INL and U. Minho), Opened a discussion on performing theoretical analysis and simulations of hBN SPEs based on the experimental data.

-Prof. Luís Alexandre (UBI), Collaboration on implementing a machine learning solution for classification of fluorescence intermittency behaviours in hBN.

Dissemination

The student's efforts contributed to the following publications and presentations at conferences:

- NanoPT2020, NanoPT2020, online conference, September 23-24, 2020 Sept 2020: Poster Oxygen assisted monocrystalline graphene growth by chemical vapor deposition Oxygen assisted monocrystalline graphene growth by chemical vapor deposition, Vitor Silva, Tiago Queirós, Ivo Colmiais, George Junior, Chun-Da Liao, Pedro Alpuim.

- FOM2021, Kinetics of DNA hybridisation observed on single molecule level using Graphene near-field effects João Carlos Roberto de Freitas, Tiago Queirós, Agnes Purwidyantri, Pedro Alpuim, Jana B. Nieder.

-Nanophotonics of 2D Materials 2021, Benasque (Spain), Tiago Queirós, Pedro Alpuim, Jana B. Nieder.

-Flashtalk at INL symposium 2020 (ranked in the top 4 best presentations).

Participation in seminars and conferences:

I attended the following seminars and conferences:

- CarbOnlineHagen 2020-Graphene growth and Carbon technologies (8 40 minute seminars);

-Technology Unites Global summit- MEMS & Imaging Sensors Forum (3h session);

-QPI Lectures- Pascale Senellart/ Pablo Jarillo-Herrero /Christian Schneider/ Chunhui Du/ Andrew Childs/ Päivi Törmä/ Carlton M. Caves/ Igor Aharonovich/ Tim Hugo Taminiau/ Sophia Economou(10 1 hour Seminars);

The student also contributed to scientific outreach activities:

-UPA Digital, Presenting Engineering Physics to secondary school students (2020/2021 Wed 5/05, 15:30-16:30).

References:

1. Aharonovich I, Englund D, Toth M. Solid-state single-photon emitters. *Nat Photonics*. 2016;10(10):631-641. doi:10.1038/nphoton.2016.186
2. Lee H, Paeng K, Kim IS. A review of doping modulation in graphene. *Synth Met*. 2018;244(March):36-47. doi:10.1016/j.synthmet.2018.07.001
3. Li W, Chen B, Meng C, et al. Ultrafast all-optical graphene modulator. *Nano Lett*. 2014;14(2):955-959. doi:10.1021/nl404356t
4. Zhao X, Li L, Zhao M. Lattice match and lattice mismatch models of graphene on hexagonal boron nitride from first principles. *J Phys Condens Matter*. 2014;26(9). doi:10.1088/0953-8984/26/9/095002
5. Grosso G, Moon H, Lienhard B, et al. Tunable and high-purity room temperature single-photon emission from atomic defects in hexagonal boron nitride. *Nat Commun*. 2017;8(1):1-8. doi:10.1038/s41467-017-00810-2
6. Wrachtrup J. 2D materials: Single photons at room temperature. *Nat Nanotechnol*. 2016;11(1):7-8. doi:10.1038/nnano.2015.265

7. Ruiz I, Wang W, George A, Ozkan CS, Ozkan M. Silicon Oxide Contamination of Graphene Sheets Synthesised on Copper Substrates via Chemical Vapor Deposition. *Adv Sci Eng Med*. 2014;6(10):1070-1075. doi:10.1166/asem.2014.1615

8. Cho SY, Kim MS, Kim M, et al. Self-assembly and continuous growth of hexagonal graphene flakes on liquid Cu. *Nanoscale*. 2015;7(30):12820-12827. doi:10.1039/c5nr03352g

9. Backes C, Abdelkader AM, Alonso C, et al. Production and processing of graphene and related materials. *2D Mater*. 2020;7(2). doi:10.1088/2053-1583/ab1e0a

10. Nasr Esfahani A, Malcolm AJ, Xu L, et al. Ultra-thin films of solution-exfoliated hexagonal boron nitride by Langmuir deposition. *J Mater Chem C*. 2020;8(39):13695-13704. doi:10.1039/d0tc02933e

11. Topsakal M, Aahin H, Ciraci S. Graphene coatings: An efficient protection from oxidation. *Phys Rev B - Condens Matter Mater Phys*. 2012;85(15). doi:10.1103/PhysRevB.85.155445

12. Liu Z, Gong Y, Zhou W, et al. Ultrathin higherature oxidation-resistant coatings of hexagonal boron nitride. *Nat Commun*. 2013;4(May):1-8. doi:10.1038/ncomms3541

13. Stern HL, Wang R, Fan Y, et al. Spectrally Resolved Photodynamics of Individual Emitters in Large-Area Monolayers of Hexagonal Boron Nitride. *ACS Nano*. 2019;13(4):4538-4547. doi:10.1021/acsnano.9b00274

14. Koperski M, Nogajewski K, Potemski M. Single photon emitters in boron nitride: More than a supplementary material. *Opt Commun*. 2018;411:158-165. doi:10.1016/j.optcom.2017.10.083

15. Sontheimer B, Braun M, Nikolay N, Sadzak N, Aharonovich I, Benson O. Photodynamics of quantum emitters in hexagonal boron nitride revealed by low-temperature spectroscopy. *Phys Rev B*. 2017;96(12):1-5. doi:10.1103/PhysRevB.96.121202

16. Li X, Shepard GD, Cupo A, et al. Nonmagnetic Quantum Emitters in Boron Nitride

with Ultranarrow and Sideband-Free Emission Spectra. *ACS Nano*. 2017;11(7):6652-6660. doi:10.1021/acsnano.7b00638

17. Malard LM, Pimenta MA, Dresselhaus G, Dresselhaus MS. Raman spectroscopy in graphene. *Phys Rep*. 2009;473(5-6):51-87. doi:10.1016/j.physrep.2009.02.003

18. Mendelson N, Xu ZQ, Tran TT, et al. Engineering and Tuning of Quantum Emitters in Few-Layer Hexagonal Boron Nitride. *ACS Nano*. 2019;13(3):3132-3140. doi:10.1021/acsnano.8b08511

19. Fröch JE, Hwang Y, Kim S, Aharonovich I, Toth M. Photonic Nanostructures from Hexagonal Boron Nitride. *Adv Opt Mater*. 2019;7(4):1-6. doi:10.1002/adom.201801344

20. Li C, Xu ZQ, Mendelson N, Kianinia M, Toth M, Aharonovich I. Purification of single-photon emission from hBN using post-processing treatments. *Nanophotonics*. 2019;8(11):2049-2055. doi:10.1515/nanoph-2019-0099

21. Matthew A. Feldman, Claire E. Marvinney, Alexander A. Puretzky and BJL. Evidence of photochromism in a hexagonal boron nitride single-photon emitter. *Optica*. 2021;8(1):1-5.

22. Comtet J, Glushkov E, Navikas V, et al. Wide-Field Spectral Super-Resolution Mapping of Optically Active Defects in Hexagonal Boron Nitride. *Nano Lett*. 2019;19(4):2516-2523. doi:10.1021/acs.nanolett.9b00178

23. Bharadwaj P, Novotny L. Robustness of quantum dot power-law blinking. *Nano Lett*. 2011;11(5):2137-2141. doi:10.1021/nl200782v

24. Haase M, Hübner CG, Reuther E, Herrmann A, Müllen K, Basché T. Exponential and power-law kinetics in single-molecule fluorescence intermittency. *J Phys Chem B*. 2004;108(29):10445-10450. doi:10.1021/jp0313674

25. Gao S, Chen HY, Bernardi M. Radiative properties of quantum emitters in boron nitride from excited state calculations and Bayesian analysis. *npj Comput Mater*. 2021;7(1):1-21. doi:10.1038/s41524-021-00544-2

26. Nguyen M, Kim S, Tran TT, et al. Nanoassembly of quantum emitters in hexagonal boron nitride and gold nanospheres. *Nanoscale*. 2018;10(5):2267-2274.

doi:10.1039/c7nr08249e

27. Ziegler J, Klaiss R, Blaikie A, Miller D, Horowitz VR, Alemán BJ. Deterministic Quantum Emitter Formation in Hexagonal Boron Nitride via Controlled Edge Creation. *Nano Lett*. 2019;19(3):2121-2127. doi:10.1021/acs.nanolett.9b00357

28. Mendelson N, Chugh D, Reimers JR, et al. Identifying carbon as the source of visible single-photon emission from hexagonal boron nitride. *Nat Mater*. doi:10.1038/s41563-020-00850-y